Suppression of Endothelial Cell FAK Expression Reduces Pancreatic Ductal Adenocarcinoma Metastasis after Gemcitabine Treatment

Marina Roy-Luzarraga[1], Louise E. Reynolds[1], Beatriz de Luxán-Delgado[1], Oscar Maiques[1], Laura Wisniewski[1], Emma Newport[1], Vinothini Rajeeve[1], Rebecca J.G. Drake[1], Jesús Gómez-Escudero[1], Frances M. Richards[2], Céline Weller[3], Christof Dormann[3], Ya-Ming Meng[4], Peter B. Vermeulen[5], Dieter Saur[6], Victoria Sanz-Moreno[1], Ping-Pui Wong[4], Cyrill Géraud[3], Pedro R. Cutillas[1], and Kairbaan Hodivala-Dilke[1]

ABSTRACT

Despite substantial advances in the treatment of solid cancers, resistance to therapy remains a major obstacle to prolonged progression-free survival. Pancreatic ductal adenocarcinoma (PDAC) is one of the most aggressive cancers, with a high level of liver metastasis. Primary PDAC is highly hypoxic, and metastases are resistant to first-line treatment, including gemcitabine. Recent studies have indicated that endothelial cell (EC) focal adhesion kinase (FAK) regulates DNA-damaging therapy–induced angiocrine factors and chemosensitivity in primary tumor models. Here, we show that inducible loss of EC-FAK in both orthotopic and spontaneous mouse models of PDAC is not sufficient to affect primary tumor growth but reduces liver and lung metastasis load and improves survival rates in gemcitabine-treated, but not untreated, mice. EC-FAK loss did not affect primary tumor angiogenesis, tumor blood vessel leakage, or early events in metastasis, including the numbers of circulating tumor cells, tumor cell homing, or metastatic seeding. Phosphoproteomics analysis showed a downregulation of the MAPK, RAF, and PAK signaling pathways in gemcitabine-treated FAK-depleted ECs compared with gemcitabine-treated wild-type ECs. Moreover, low levels of EC-FAK correlated with increased survival and reduced relapse in gemcitabine-treated patients with PDAC, supporting the clinical relevance of these findings. Altogether, we have identified a new role of EC-FAK in regulating PDAC metastasis upon gemcitabine treatment that impacts outcome.

Significance: These findings establish the potential utility of combinatorial endothelial cell FAK targeting together with gemcitabine in future clinical applications to control metastasis in patients with pancreatic ductal adenocarcinoma.

[1]Barts Cancer Institute—A CR-UK Center of Excellence, Queen Mary University of London, John Vane Science Center, Charterhouse Square, London, United Kingdom. [2]Translational Medicine Operations, Astrazeneca Oncology, Darwin Building, Cambridge Science Park, Milton Road, Cambridge, United Kingdom. [3]Department of Dermatology, Section of Clinical and Molecular Dermatology, Venereology and Allergology, University Medical Center and European Center for Angioscience, Medical Faculty Mannheim, Heidelberg University, Mannheim, Germany. [4]Guangdong Provincial Key Laboratory of Malignant Tumor Epigenetics and Gene Regulation, Guangdong-Hong Kong Joint Laboratory for RNA Medicine, Sun Yat-sen Memorial Hospital, Sun Yat-sen University, Guangzhou, China. [5]Department of Oncological Research, Translational Cancer Research Unit, Oncology Center GZA—GZA Hospitals St. Augustinus and University of Antwerp, Antwerp, Belgium. [6]Division of Translational Cancer Research, German Cancer Research Center (DKFZ) and German Cancer Consortium (DKTK), Heidelberg and Chair of Translational Cancer Research and Institute for Experimental Cancer Therapy, Klinikum rechts der Isar, School of Medicine, Technische Universität München, München, Germany.

Introduction

The lung and liver are common sites of metastasis for pancreatic ductal adenocarcinoma (PDAC), the fourth leading cause of cancer-related death, with a dire 8% five-year survival rate (1). Most patients with PDAC are not eligible for surgical resection as they present with advanced metastatic disease at time of diagnosis. Although treatment with nucleoside analogues, including gemcitabine, remains a part of the first-line chemotherapy treatment for PDAC, resistance to gemcitabine is still a significant limitation for treatment efficacy and contributes to the associated poor prognosis (2). Thus, new therapeutic strategies are needed.

The tumor microenvironment has been described previously to play key roles in modulating chemotherapy resistance and subsequent disease progression (3). Apart from their role in the development of new blood vessels that are essential for oxygen and nutrient delivery to the tumor, tumor endothelial cells (EC) and their angiocrine-secreted factors constitute a vascular niche essential for initiation, growth, and progression of cancer (4, 5). For example, primary tumor cells induce activation of EC-Notch 1 in pre-metastatic sites, which induces over-expression of angiocrine-senescent factors that facilitate extravasation of malignant cells and metastasis (6). In breast and colorectal cancer, EC-Jagged-1 not only induces a stem-like phenotype but also enhances pro-metastatic traits (7). EC-secreted EGF has been shown to also induce both EMT and acquisition of a stem-like phenotype in head and neck cancer cells (8). The cross-talk between lymphoma cells and neighboring ECs affects chemotherapy response. FGF4 produced by B-cell lymphoma cells upregulates EC-Jagged 1 that in turn induces

activation of Notch2–Hey1 pathway in lymphoma cells. This FGF4–Jag1–Notch2 loop enhances lymphoma aggressiveness and chemoresistance (9). DNA-damaging therapy induces secretion of IL-6 and Timp-1 from ECs via NF-κB pathway in the thymus. Release of these angiocrine factors upon DNA-damage in Burkitt's lymphoma, produces a chemoresistant niche that induces the survival of a minimal residue of tumor burden responsible for cancer relapse (10).

Focal adhesion kinase (FAK) is a member of the nonreceptor protein tyrosine kinase family. FAK is ubiquitously expressed and signals downstream of integrins and growth factor receptors in its role as a coordinator of cell migration and proliferation (11).

Loss of FAK in tumor ECs reduces tumor angiogenesis initiation thus affecting tumor growth (12). In addition, loss of EC-FAK regulates tumor metastasis to the lung via the control of phosphorylation of VE-cadherin (13). In this study, conditional EC-FAK kinase dead (KD) knockin mice were used to show that loss of EC-FAK kinase activity prevents VEGF-stimulated tumor cell extravasation and spontaneous metastasis without impacting primary tumor growth (13). Most recently, tumor angiogenesis has been shown to be differentially regulated by EC FAK tyrosine-397 and -861 phosphorylation (14) and EC-FAK kinase activity is involved in regulating doxorubicin sensitivity (15).

Several lines of evidence have indicated essential roles for FAK in the production of secreted paracrine signals (16). Most relevant here, EC-FAK regulates angiocrine-derived paracrine factors that control a chemoprotective tumor cell niche (17). Inducible loss of EC-FAK in established tumors does not affect tumor angiogenesis but does sensitize malignant cells to DNA-damaging therapies. In melanoma and Lung Lewis carcinoma subcutaneous murine models treated with doxorubicin, a significant reduction in tumor growth was observed upon EC-FAK depletion compared with treated EC-FAK^{WT} mice (17), suggesting that loss of EC-FAK expression together with doxorubicin treatment generates a niche that sensitizes malignant cells to doxorubicin. However, the role of EC-FAK in chemosensitization and metastatic PDAC is unknown.

Here, we establish that loss of EC-FAK can reduce liver or lung metastases in gemcitabine-treated mice without affecting PDAC primary tumor growth.

Materials and Methods

Genetic modified mouse models

All animal procedures described previously in this project were approved by the UK Home Office and carried out according to the ARRIVE guidelines. The inducible mouse model *Pdgfb-iCre^{ERT}; Fak$^{fl/fl}$* has been previously described and characterized (12). The *Pdx1-flp; frt-STOP-frt-Kras$^{G12D/+}$; p53$^{frt/+}$* (KPF) mice (18) were bred with the *Pdgfb-iCre^{ERT}; Fak$^{fl/fl}$* mice to generate the spontaneous model *Pdx1-flp; frt-STOP-frt-Kras$^{G12D/+}$; p53$^{frt/+}$; Pdgfb-iCre^{ERT}; Fak$^{fl/fl}$*. Genotyping of the mice was performed as described previously (12, 18).

8661 and TB32048 pancreatic cancer cell lines

For the 8661 cell line (gift from Prof. Dieter Saur, Technische Universitat München, München, Germany), primary PDAC cell cultures were isolated from autochthonous PDAC and cultured as described previously (19). All cells used were cultivated for less than 30 passages, authenticated by genotyping, validated by a specific PCR that detects the recombined LSL allele of KrasG12D, and tested regularly for *Mycoplasma* contamination by PCR (20).

KrasLSL.G12D$^{/+}$; p53R172H$^{/+}$; PdxCretg$^{/+}$ (KPC)-derived TB32048 murine pancreatic cancer cell line (derived from C57/BL6) was obtained from Prof. David Tuveson (Cold Spring Harbor, Cold Spring Harbor, NY) and treated as for the 8661 cell line.

Pancreatic orthotopic injections

A total of 1×10^3 8661 or TB32048 pancreatic cancer cell lines were injected into the pancreas of syngeneic immunocompetent *Pdgfb-iCre^{ERT}; Fak$^{fl/fl}$* mice. Briefly, mice were anesthetized by inhalation anesthesia (2% isoflurane) and given analgesia subcutaneously. An incision in the left flank of the skin followed by an incision in the muscular layer using blunt-ended scissors was made to carefully reveal the spleen and pancreas. Cells were injected into the tail of the pancreas in 10 μL of 1:1 Matrigel and PBS, using a Hamilton syringe. After positioning the organs back inside the body cavity, the muscular layer and skin incision were closed with sutures and surgical staples, respectively. Animals were monitored until complete recovery.

Intrasplenic injections

Pdgfb-iCre^{ERT}+; Fak$^{fl/fl}$ and *Pdgfb-iCre^{ERT}−; Fak$^{fl/fl}$* mice were anaesthetized by inhalation anesthesia (2% isoflurane) and given analgesia subcutaneously. An incision in the left flank of the skin followed by an incision in the muscular layer using blunt-ended scissors was made to carefully reveal the spleen on the surface of the body during surgery. A total of 4×10^5 8661 pancreatic cancer cells in 30 μL of PBS were injected into the spleen using an insulin syringe. After the injection, a cotton bud was pressed onto the injection site for at least a minute to avoid any leakage or bleeding. The spleen was repositioned back inside the body, the muscular layer sutured and the skin incision closed using surgical staples. Animals were monitored to complete recovery. For 7-day colonization experiments, a splenectomy was performed 5 minutes after injection using a cauterizer to avoid primary tumor formation in the spleen. For short-term experiments (2 and 48 hours after injection) the spleen was not removed.

In vivo treatment strategy

Upon orthotopic injections, mice were given a soy-free diet (Harlan) to reduce estrogen levels and increase tamoxifen sensitivity. At day 12 after tumor cell inoculation, tumors were palpable and imaged by MRI (Bruker ICON 1T MRI system, Bruker) to confirm tumor formation. Mice with no tumor at this stage were discarded from the study and mice with tumors sized between 30 and 100 mm^3 were treated intraperitoneally (IP) with 100 μL of 10 mg mL^{-1} tamoxifen (Sigma T5648) for two consecutive days. After the last tamoxifen injection all mice were fed a tamoxifen-containing diet (TAM400, Harlan). Mice were then injected IP with 75 mg kg^{-1} of gemcitabine (Gemzar), or saline as a negative control, every other day for three days. Tumor growth was monitored by MRI every week at experimental days 19, 23, and 26.

For the spontaneous *Pdx1-flp; frt-STOP-frt-Kras$^{G12D/+}$; p53$^{frt/+}$; Pdgfb-iCre^{ERT}; Fak$^{fl/fl}$* model, mice were monitored for evidence of a palpable tumor. These mice were then imaged by MRI or Ultrasound (Vevo 2100 system) to assess tumor size, and only mice with tumors sized between 50 and 350 mm^3 were used for the experiment. Experimental mice were given two tamoxifen injections intraperitoneally followed by tamoxifen diet and subsequently treated or not with gemcitabine (75 mg kg^{-1}) every other day for three days, as described previously. All mice were monitored for disease symptoms and killed at humane end points. For model characterization, nontumor burdened animals were treated IP with tamoxifen for two consecutive days. 48 hours after treatment tissue from pancreas, liver, kidney, heart and lung was processed and hematoxylin and eosin (H&E)–stained for histopathological assessment.

For the intrasplenic model, before tumor cell injections, mice were given two tamoxifen injections intraperitoneally followed by tamoxifen diet and gemcitabine treatment or not (75 mg kg^{-1}) every other day for three days.

Tumor progression and metastasis assessment

Tumor growth over time and tumor size at day 26 was calculated by MRI images using VivoQuant software. Final tumor volumes (FV) were measured at end point (day 41 for untreated cohort and day 44 for the gemcitabine-treated group) using a caliper and calculated: FV = length × width × depth. Metastatic burden was assessed histologically by H&E staining and metastasis size was quantified using Pannoramic Viewer Software and viewed with 3D HISTECH software. The scanner produced images by tiling high-resolution fields together.

Gemcitabine delivery

Pdgfb-iCre^ERT; Fak^fl/fl mice were orthotopically injected with 8661 tumor cells and treated with tamoxifen and gemcitabine as described previously in "*In vivo* treatment strategy." At day 28 after injection, mice were injected intraperitoneally with a high dose of gemcitabine (125 mg kg^{-1}) and culled after 15 minutes. Tumors and livers were collected and three pieces of at least 10 mg of each organ per mouse were snap-frozen in liquid nitrogen and stored at −80°C before analysis by LC-MS/MS by the CRUK Cambridge Institute PK/Bioanalytics core facility. Digestion and sample preparation for LCMS analysis as well as the bioanalytic study for Gemcitabine (dFdC), and 2′-deoxy-2′,2′-difluorouridine (dFdU) detection was performed as previously described (21).

Circulating tumor cells

Pdgfb-iCre^ERT; Fak^fl/fl mice were orthotopically injected with 8661 tumor cells and treated with tamoxifen and gemcitabine as described previously in "*In vivo* treatment strategy." At day 41 after injection, blood was removed by cardiac puncture as an end point procedure. Plasma was discarded and the blood transferred to a 15 mL falcon tube for red blood cell lysis. For red blood cell lysis, 9 mL of 1x Red blood cell lysis solution was added to the blood, mixed and incubated for 10 minutes at room temperature. Samples were then centrifuged at 400 × *g* for 8 minutes at room temperature. The resulting pellet was washed with PBS and used for subsequent flow cytometry analysis. The eBioscience Foxp3 /Transcription Factor Staining Buffer Set (Thermo Fisher Scientific; 00–5523–00) was used for the intracellular staining of Pdx-1 (Abcam ab47383), diluted 1:100, and CD45-Pacific Blue–conjugated antibody (BioLegend, 103125), 1:200 dilution, following the manufacturers' instructions. Anti-Goat Alexa Fluor 647 (Invitrogen; 1:100 dilution) was used as secondary antibody and Zombie Green viability dye to stain dead cells (Zombie Green Fixable Viability kit, BioLegend). For flow cytometry analysis, samples were run on the BD LSRFortessa flow cytometer (BD Biosciences) using the BD Cell Quest Pro software. Blood from a nontumor-bearing mouse, and 8661 tumor cells were processed in parallel and were used as negative and positive controls, respectively, for the gating strategy.

Homing experiment

8661 pancreatic cancer cells were labeled with GFP using Cell-Tracker Green CMFDA (Invitrogen C7025) following the manufacturers' instructions, and injected intrasplenically into *Pdgfb-iCre^ERT; Fak^fl/fl* mice previously treated as described in "*In vivo* treatment strategy." 2 hours after injection, livers were collected and digested for subsequent flow cytometry analysis. First, livers were minced and incubated with collagenase P (Roche 11213865001) for 10 minutes at

37°C and Trypsin/EDTA for 3 minutes at 37°C. Cell suspension was filtered using a 70-μm strainer and centrifuged for 5 minutes at 1,200 rpm. Cell pellets were resuspended in ACK lysis buffer (Gibco A10492–01) and incubated for 1 minute at room temperature for red blood cell lysis. After washing with DMEM medium, pellets were then resuspended with FACS buffer filtered through a 70-μm strainer and stained with 3 μmol/L DAPI. Samples were run on the flow cytometer BD LSRFortessa (BD Biosciences) using the BD Cell Quest Pro software. Liver cell suspension from a noninjected animal and GFP labeled 8661 tumor cells were used as negative and positive controls, respectively. The percentage of GFP-positive cells in the DAPI-negative population was calculated per liver sample.

Seeding and colonization experiment

Pdgfb-iCre^ERT; Fak^fl/fl mice were injected intrasplenically with 8661 tumor cells, previously treated as in "*In vivo* treatment strategy." Livers were collected at 48 hours after injection to assess seeding and at 7 days after injection to assess colonization. Livers were fixed in 10% formalin overnight and transferred to 70% ethanol. Tumor cell seeding and colonization was assessed by Pdx-1 staining of liver sections.

Hoechst leakage

Pdgfb-iCre^ERT; Fak^fl/fl mice were orthotopically injected with 8661 tumor cells and treated with tamoxifen and gemcitabine as described previously in the "*In vivo* treatment strategy" section. At day 28 mice were injected via the tail vein with 100 μL of Hoechst at 4 μg mL^{-1} (Thermo Fisher Scientific 33342; Mw 561.93 kDa) dye and culled 1 minute after injection. Frozen sections were stained with CD31 conjugated with PE (BioLegend 102498), mounted with Vectashield Antifade Mounting Media without DAPI (Vector Laboratories) and scanned using the Nano Hamamatsu Nano Zoomer 2.0-RS slide scanner. Hoechst and CD31-positive area were measured by ImageJ software and blood vessel leakage was calculated by the ratio between both areas.

Immunostaining

H&E and Pdx-1 staining (Abcam 47267) was performed using the Ventana Discovery XT (Roche Diagnostics). For endomucin (Santa Cruz Biotechnology sc65495, 1:250 dilution) and Ki67 (Abcam 16667, 1:200 dilution) staining, paraffin sections were deparaffinized in 2 changes of xylene, 10 minutes each, then hydrated in 2 changes of 100% ethanol for 5 minutes followed by 80%, 70%, and 50% ethanol, 2 minute each before 2 minutes in distilled water. Sodium Citrate Buffer (10 mmol/L, pH6) was heated in the microwave for 10 minutes. Slides were then immersed in preheated Sodium Citrate Buffer for 10 minutes and cooled on the bench for 20 minutes. Slides were then washed twice with PBS and endogenous peroxidase was blocked with 3% H$_2$O$_2$ in methanol. Slides were washed twice with PBS and once with PBS 0.1% Tween (PBS-T) followed by blocking with horse serum for 1 hour at room temperature. Slides were incubated overnight with primary antibody diluted in blocking buffer overnight at 4°C. The slides were then washed three times with PBS-T before incubating with the secondary anti-rat biotinylated antibody (be-9401 Vector Laboratories, 1:200 dilution) in blocking buffer for 40 minutes at room temperature. Slides were washed three times with PBS-T and incubated with ABC working solution (Vectastain ABC kit PK-6200 Universal) for 30 minutes at room temperature. The reaction was developed using DAB substrate and slides were counterstained with hematoxylin. Slides were dehydrated then mounted with DPX mounting media. Stained sections were scanned (Panoramic 250 Flash) and visualized using the Pannoramic Viewer software. Proliferative

index was calculated by dividing positive DAB nuclei by total hematoxylin-stained nuclei using Visiopharm Quantitative Digital pathology software.

For Glut-1 (Thermo Fisher Scientific, 37783), paraffin sections were deparaffinized in 2 changes of xylene, 10 minutes each, then hydrated in 2 changes of 100% ethanol for 5 minutes followed by 80%, 70%, and 50% ethanol, 2 minute each before 2 minutes in distilled water. Slides were incubated at 60°C for 20 minutes and then subjected to antigen retrieval using antigen unmasking solution, Citric Acid Base (1:100; H-3300; Vector Laboratories) at 110°C for 6 minutes in a Decloaking Chamber NxGen (Biocare Medical). Samples were blocked with Dual Endogenous Enzyme-Blocking Reagent (Dako) for 10 minutes and then incubated with primary antibodies (1:500 dilution) for 40 minutes at room temperature, washed and then incubated with rabbit (1:200; BA-1000; Vector Laboratories) or mouse (1:200; BA-9200; Vector Laboratories) biotinylated secondary antibody for 30 minutes at room temperature. Signal was then amplified using Vectastain ABC HRP Elite kit (PK-6100; Vector Laboratories) for 20 minutes at room temperature and the reaction was developed using VIP substrate (SK-4600, Vector Laboratories) for 10 minutes at room temperature. Stainings were counterstained with hematoxylin. Both tumor and liver sections were scanned using the NanoZoomer S210 slide scanner. Staining quantification was performed using QuPath 0.1.2. The entire whole-section images were analyzed performing positive cell detection.

For FAK/endomucin sequential staining, paraffin-fixed sections were stained as described previously (22). Briefly, tumor tissues were formalin-fixed paraffin-embedded (FFPE) as per standard protocols. Sections of 4-μm thickness were heated at 60°C for 1 hour and then incubated in xylene and ethanol series, with 2×5 minutes H_2O_2/ethanol incubations to block endogenous peroxidase. Antigen retrieval was performed in Antigen Unmasking Solution (H-3300, Vector Laboratories) using a pressure cooker system (110°C for 10 minutes). Samples were washed in Dako Wash Buffer (S3006) and endogenous biotin was blocked by incubating for 30 minutes, with each solution from the Avidin/Biotin Blocking Kit (SP2001, Vector Laboratories), before primary antibody incubation (1 hour, 1:50 anti-FAK, CST 3285), diluted in Antibody Diluent Reagent Solution (003218, Invitrogen/Thermo Fisher Scientific). Samples were washed and incubated with biotinylated secondary antibody, diluted in same antibody diluent solution (goat anti-rabbit, 1:200, Vector Laboratories) for 30 minutes. Signal was amplified using the Vectastain ABC HRP kit (PK-4000, Vector Laboratories) for 20 minutes and the reaction was developed using VIP peroxidase substrate solution (SK-4600, Vector Laboratories) for 10 minutes. All incubations were carried out at room temperature. Slides were counterstained with hematoxylin and mounted using DPX mounting medium (06522–500ML, Sigma). Slides were scanned using the NanoZoomer S210 slide scanner. The next day, slides were processed using the same procedure, using anti-endomucin primary antibody (40 minutes, 1:200, sc-558) and biotinylated goat anti-rat secondary antibody (1:200, Vector Laboratories, 1 hour); signal amplification, mounting, and imaging was repeated as before. Slide images were aligned using QuPath software v.0.2.0m7 and double staining assessed qualitatively in FIJI v1.52p, using 3 fields of view per slide at ×10 magnifications that were endomucin-positive stained, a score between 0 and 1 was assigned per field of view whereby $0 =$ all vessels FAK$^-$, $1 =$ all vessels FAK$^+$.

For colocalization analysis, images for PDX-1 and vimentin (Cell Signaling Technology, 1:700; 5741) markers were aligned in FIJI v1.52p using TrackEM2 module. Next, color deconvolution was performed using AEC-hematoxylin vectors and a composite was created using channel-2 (red) for each staining. The composite was adjusted inverting the LUT for each marker and was given a pseudo-color (Vimentin, green; PDX-1, red; nuclei, blue). Composite images were analyzed in Qupath using cell detection tool, to quantify the percentage of double-positive cells.

For cleaved caspase-3 (CC3) and PECAM immunofluorescence, tumors were dissected and snap-frozen. Frozen tumor sections were air-dried then rehydrated for 5 minutes in PBS. Sections were fixed with ice-cold acetone for 10 minutes and washed once with PBS. Sections were blocked for 30 minutes at room temperature with 1%BSA/PBS followed by incubation with CC3 (Cell Signaling Technology, 9664) and PECAM (Agilent Dako, clone JC70A, 76539) overnight at 4°C (both diluted 1:100 in PBS). The following day sections were washed 3 times with PBS then incubated with the relevant fluorescent-conjugated antibody diluted 1:100 in 1% BSA/PBS for 1 hour at room temperature. This was followed by three PBS washes and one wash with water containing 1:10,000 dilution DAPI (Molecular Probes). Sections were mounted with Prolong Gold anti-fade solution.

Histological staining

FFPE liver tissue sections (3 μm) were deparaffinized and rehydrated according to standard protocols. Histological staining using H&E, Picrosirius red, periodic acid-Schiff (PAS), and Prussian blue were conducted according to standard protocols.

Cell culture

Cell culture was carried out under sterile conditions in a tissue culture hood and cells were grown at 37°C and 5% CO_2. 8661 and TB32048 pancreatic cancer cells were grown in DMEM (Sigma D6429) with 10% FBS (Sigma F9665) and 1% penicillin–streptomycin (P4333 Sigma).

Western blotting

FAK^{WT} and FAK^{KO} primary lung ECs were isolated as described previously (23). Protein was isolated by lysing cells in RIPA buffer containing protease and phosphatase inhibitors (1:100 dilution, Roche) at 4°C for 10 minutes followed by centrifugation for 10 minutes at 4°C to pellet cell debris. For analysis of protein levels, lysates were subjected to SDS-PAGE and transferred to nitrocellulose membranes (Amersham Biosciences) for Western blotting. Blots were probed for FAK (1:1,000 dilution, 3285, Cell Signaling Technology), Phospho-PAK1/2 and PAK1 (both 1:1,000 dilution, 2601 and 2602, Cell Signaling Technology), Phospho–β-Catenin (Ser675; 1:1,000, 4176, Cell Signaling Technology), HSC70 (1:5,000 dilution, V7C7, Santa Cruz Biotechnology), and tubulin (1:2,000, T5168, Sigma) for the loading control. Densitometric readings of band intensities were obtained using the ImageJ software.

Statistical analysis

All after analysis studies from the *in vivo* experiments were carried out in a blinded manner. Statistical analyses were performed using GraphPad Prism 8.0 software. Kolmogorov–Smirnov and Shapiro–Wilk tests were used to assess normality. For paired comparisons with normal distributed data, a Student *t* test was used. Nonparametric Mann–Whitney test was used when data showed non-normal distribution. Two-way ANOVA was used for multiple comparisons and χ^2 test for incidence analysis. Statistical significance was considered when a *P* value was of <0.05.

Cumulative survival probabilities were estimated using the Kaplan–Meier method, and differences between survival rates in

murine models were tested for significance using the Gehan–Breslow–Wilcoxon test.

Phosphoproteomics analysis

Protein extraction and trypsin digestion was performed as previously described (24, 25). 7.5×10^5 FAK^{WT} or FAK^{KO} mouse lung ECs (MLEC) grown in MLEC media (40% Ham's F12 with Glutamax, 40% DMEM with 1g/l glucose, Glutamax and pyruvate, 20% FBS, 12.5 mg/L of EC supplements, 1% penicillin/streptavidin and 2% Glutamax) plus 10 nmol/L tamoxifen, were seeded in 10-cm dishes pre-coated with 0.1% gelatin in PBS with 22.5 μg/mL collagen and 5 μg/mL fibronectin. The day after, the media were replaced with or without 60 nmol/L gemcitabine for both cell lines, and cells were grown in normoxia or hypoxia (0.8% O_2) for 48 hours. Briefly, cells were washed twice with ice-cold PBS supplemented with phosphatase and protease inhibitors (1 mmol/L Na_3VO_4 and 1 mmol/L NaF) and lysed (either in normoxia or hypoxia) with a denaturing buffer with phosphatase and protease inhibitors (20 mmol/L HEPES pH 8.0, 8 mol/L urea, 1 mmol/L Na_3VO_4, 1 mmol/L NaF, 2.5 mmol/L $Na_4P_2O_7$, 1 mmol/L ß-glycerol-phosphate). Cell lysates were further homogenized by sonication and insoluble material was removed by centrifugation at 13,000 × g for 10 minutes at 4°C. Protein concentration in the supernatants was calculated using Pierce BCA Protein Assay Kit (Thermo Fisher Scientific). 250 μg of protein was reduced and alkylated by sequential incubation with 10 mmol/L dithiothreitol and 16.6 mmol/L iodoace-tamide for an hour. Urea concentration was diluted to below 2 mol/L with 20 mmol/L HEPES (pH 8.0), trypsin beads (50% slurry of TLCK-trypsin; Thermo Fisher Scientific; 20230) were added and samples were incubated on a thermoshaker for 18 hours at 37°C. Trypsin beads were removed by centrifugation at 2,000 × g for 5 minutes at 4°C. Peptide solutions were desalted using 10-mg OASIS-HLB cartridges. Cartridges were activated with acetonitrile (ACN; 100%) and equilibrated with washing solution (1% ACN, 0.1% TFA). After loading the samples, washing solution was applied to cartridges. Peptides were eluted with glycolic acid buffer (1 mol/L glycolic acid, 50% ACN, 5% TFA).

To enrich phosphopeptides, sample volumes were normalized using glycolic acid buffer (1 mol/L glycolic acid, 80% ACN, 5% TFA), 50 μL of TiO_2 beads (50% slurry in 1% TFA; Hichrom) were added to the peptide mixture, incubated for 5 minutes at room temperature with agitation and centrifuged for 30 seconds at 1,500 × g. For each sample, the supernatant was transferred to fresh tubes and stored on ice and the pelleted TiO_2 was loaded into an empty PE-filtered top tip (Glygen) prewashed with ACN and packed by centrifugation at 1,500 × g for 3 minutes. After loading the remaining volume of the supernatant by centrifugation at 1,500 × g for 3 minutes, top tips were sequentially washed by 3 minutes centrifugation at 1,500 × g with glycolic acid buffer, 100 mmol/L ammonium acetate in 25% ACN and twice with 10% ACN. For phosphopeptide recovery, peptides were eluted 4 times by 3 minutes centrifugation at 1,500 × g with 5% NH_4OH. Eluents were dried in a speed vac and peptide pellets stored at −80°C.

For LC-MS/MS analysis, phosphopeptides were reconstituted in 13 μL of reconstitution buffer (97% H_2O, 3% ACN, and 0.1% TFA, 50 fmol/μL-1 enolase peptide digest) and sonicated for 2 minutes at room temperature. Phosphopeptides were analyzed using nano flow ultimate 3000 RSL nano instrument, coupled on-line to a Q-Exactive plus mass spectrometer (Thermo Fisher Scientific). Gradient elution was from 3% to 35% buffer B in 90 minutes at a flow rate 250 nL/min with buffer A used to balance the mobile phase (buffer A was 0.1% formic acid in water and B was 0.1% formic acid in ACN). The mass spectrometer was controlled by Xcalibur software (version 4.0) and operated in the positive mode. The spray voltage was 1.95 kV and the capillary temperature was set to 255°C. The Q-Exactive plus was operated in data-dependent mode with one survey MS scan followed by 15 MS/MS scans. The full scans were acquired in the mass analyzer at 375—1,500 m/z with the resolution of 70,000, and the MS/MS scans were obtained with a resolution of 17,500.

Peptide identification and quantification

For peptide identification, MS raw files were converted into Mascot Generic Format using Mascot Distiller (version 2.7.1) and searched against the SwissProt database (release September 2019) restricted to human entries using the Mascot search daemon (version 2.6.0; ref. 25) with a FDR of approximately 1% and restricted to the human entries. Allowed mass windows were 10 ppm and 25 mmu for parent and fragment mass to charge values, respectively. Variable modifications included in searches were oxidation of methionine, pyro-glu (N-term) and phosphorylation of serine, threonine and tyrosine. Peptides with an expectation value of <0.05 were considered for further analysis. The mascot result (DAT) files were extracted into excel files. For peptide quantification, Pescal Software (26) was used to construct extracted ion chromatograms (XIC) for all the identified peptides across all conditions and calculating the peak heights. These peptide peak heights were then normalized to the sum of the intensities for each individual sample and the average fold change between conditions could be determined. Statistical significance between conditions was considered significant when the Student t tests produced $P < 0.05$ following Benjamini–Hochberg (BH) multiple testing correction. Kinase substrate enrichment analysis (KSEA) was performed as described before (26). Briefly, peptides differentially phosphorylated between a set of samples (at nonadjusted $P < 0.05$) were grouped into substrate sets known to be phosphorylated by a specific kinase as annotated in the PhosphoSite, Phospho.ELM, and PhosphoPOINT databases (27–29). To infer enrichment of substrate groups across sets of samples, the hypergeometric test was used followed by BH multiple testing corrections.

Conditioned medium experiments

FAK^{WT} or FAK^{KO} MLEC were grown to confluency and treated with 7.5 μg/mL mitomycin C for 2 hours at 37°C. The cells were trypsinized and replated into T25 flasks in MLEC for 24 hours. The following day, the medium was discarded and replaced with medium with 100 nmol/L gemcitabine for 48hr (based on dose–response curve data).

A total of 1×10^3 8661 cells/well were seeded into 96-well plates in DMEM + 10% FCS (Life Technologies), allowed to adhere and then the medium was replaced with Optimem. After 48 hours, MLEC conditioned medium (CM) was collected, filtered, and added to the 8661 cells. 8661 cell proliferation was assessed at day 3 after incubation with CM using the MTT assay. MLECs were trypsinized and protein extracted for Western blot analysis for phospho-PAK1 and phospho–β-catenin levels.

MTT assay

MTT powder (Invitrogen, M6494) was dissolved in PBS to make a 5 mg/mL solution (10X stock). The media were removed from the 96-well plates and a 1X MTT solution (dissolved in 8661 medium) was added to the wells. The plates were incubated at 37°C for 3 hours then the MTT solution was removed and 50 μL DMSO added to each well to solubilize the formazan. The plates were read at 570 nm with the Omega plate reader (BMG Labtech).

Human data

All human pancreatic cancer samples were collected from patients with informed consent, and all related procedures were performed with the approval of the internal review (as requested by the Declaration of Helsinki) and ethics boards of Sun Yat-Sen University memorial hospitals. Ethnics no: SYSEC-KY-KS-2019–100.

Immunostaining of human tissue

Human pancreatic cancer samples (Sun Yat-Sen memorial hospital) were obtained with signed informed consent from patients and ethical committee approval. Patients with PDAC all received gemcitabine-based treatment after surgery and their clinical responses to gemcitabine were evaluated and recorded ($n = 40$ patients), and some of these patients with their relapse information ($n = 26$ patients with PDAC). FFPE human PDAC tissues were cut into 4-mm sections and subjected to immunofluorescent staining as previously described (30). Antibodies used for immunofluorescent staining were mouse monoclonal anti-CD34 antibody against human cell surface glycoprotein (ZSGB-BIO, ZM-0046, 1:100 dilution) and rabbit monoclonal anti-FAK antibody against human or mouse (Cell Signaling Technology, 3285S, 1:100 dilution). For the immunofluorescence analysis, Alexa Fluor–conjugated secondary antibodies (Invitrogen Molecular Probes) were used to detect human antigens, and the sections were counterstained with DAPI (Sigma-Aldrich, D8417). For data analysis, the percentage of FAK negative blood vessels was calculated as the number of CD34-positive blood vessels that were negative for FAK over the total number of CD34-positive blood vessels. Patient data are expressed as those with either less, or more, than 44% of blood vessels that are FAK negative.

Data availability

The mass spectrometry proteomics data have been deposited to the ProteomeXchange Consortium via the PRIDE (31) partner repository with the dataset identifier PXD021542 and 10.6019/PXD021542.

Results

EC-FAK deletion does not affect primary PDAC tumor growth but regulates liver and lung metastasis upon gemcitabine treatment

To study the effect of EC-FAK deletion on primary tumor growth, murine pancreatic 8661 cancer cells were injected into the pancreas of both *Pdgfb-iCre^ERT -; Fak^fl/fl* and *Pdgfb-iCre^ERT +; Fak^fl/fl* (12). Once tumors were established, mice were given tamoxifen to induce FAK deletion in ECs of *Pdgfb-iCre^ERT +; Fak^fl/fl* (EC-FAK^KO) but not *Pdgfb-iCre^ERT -; Fak^fl/fl* (EC-FAK^WT) mice. Tumor burdened EC-FAK^KO and EC-FAK^WT mice were treated with gemcitabine, or saline as controls, every other day for three days. Efficient *in vivo* deletion of FAK was observed in EC-FAK^KO mice, both untreated and gemcitabine treated, when compared with EC-FAK^WT mice in the endothelium of primary tumors and liver metastatic nodules (Supplementary Fig. S1A–S1D). Primary tumor growth was monitored over time and no differences in tumor growth, final tumor volume, gross tumor appearance, morphology, tumor weight (**Fig. 1A–C**) or mouse body weight (Supplementary Fig. S1E) were observed upon EC-FAK deletion regardless of gemcitabine treatment. EC apoptosis, was not detectable by double immunostaining for cleaved caspase 3 and PECAM in primary 8661 tumors, from treated or untreated EC-FAK^WT or EC-FAK^KO mice (Supplementary Fig. S1F).

When examining metastases, both EC-FAK^WT and EC-FAK^KO mice had similar numbers of 8661 liver metastatic nodules with or without gemcitabine treatment (**Fig. 1D**), and individual metastatic liver nodule areas were similar in both genotypes (**Fig. 1E**). However, in contrast, individual liver metastatic nodule area was significantly decreased in gemcitabine treated EC-FAK^KO compared with gemcitabine EC-FAK^WT mice (**Fig. 1F**). Also in this 8661 model, although the number of lung metastases was comparable between the genotypes, there was a trend toward a reduction of individual lung metastasis area in gemcitabine treated EC-FAK^KO mice at this time point (Supplementary Fig. S1G).

Using a second murine pancreatic cancer cell line, TB32048 injected orthotopically in the pancreas, no differences in primary tumor volume, tumor weight or mouse body weight were observed between EC-FAK^WT or EC-FAK^KO mice after gemcitabine treatment (Supplementary Fig. S2A–S2C). In this model, metastasis to the lung was prevalent, but hardly any metastasis to the liver was observed. Examination of lung metastases showed a similar number of metastatic lung nodules between gemcitabine-treated mice, and a significant reduction in nodule size in EC-FAK^KO gemcitabine-treated mice (Supplementary Fig. S2D–S2F). No significant differences in primary PDAC tumor cell Ki67 staining were observed at the experimental end point of gemcitabine- or saline-treated EC-FAK^WT or EC-FAK^KO mice (Supplementary Fig. S3A and S3B).

Together, these data indicate that loss of EC-FAK can decrease metastasis area in liver and lung depending on the orthotopically injected PDAC model used.

Because epithelial–mesenchymal transition (EMT) is a key driver of metastasis, changes in metastasis could be attributed to altered EMT transition. Analysis of numbers of Pdx1^+/vimentin^+ cells showed an increase in these markers at the invasive front, compared with the tumor body, of tumors from both genotypes. This was not affected by gemcitabine treatment, suggesting that the EC-FAK^KO tumors had similar levels of EMT to EC-FAK^WT (Supplementary Fig. S3C). Levels of metastasis may also be associated with intrinsic changes in liver fibrosis, iron deposition, and metabolic zonation that occur in other liver pathologies (32). No obvious changes were observed in H&E, Sirius Red, PAS or Prussian Blue staining between pre-metastatic livers from gemcitabine-treated EC-FAK^KO and EC-FAK^WT mice, suggesting an absence of changes in liver fibrosis and iron deposition that might be responsible for the altered metastasis observed in gemcitabine treated EC-FAK^KO mice (Supplementary Fig. S4A). In addition, no changes in Glutamine synthetase (Glul) and Arginase-1 (Arg1) staining were observed between genotypes, indicating unaltered metabolic zonation (Supplementary Fig. S4B). These results suggest a role for EC-FAK in regulating PDAC metastatic, upon gemcitabine treatment, without affecting primary tumor growth or markers of changes in EMT, liver fibrosis, iron deposition or metabolic zonation.

Utility of a third model of PDAC, the genetically modified *Pdx1-flp; frt-STOP-frt-Kras^G12D/+; p53^frt/+* (KPF) mice, identifies that EC-FAK deletion enhances mean survival and decreases liver and lung metastasis after gemcitabine treatment

We next asked whether the reduction in metastatic growth in gemcitabine-treated EC-FAK^KO mice could provide a survival advantage. For this, we generated a KPF EC-FAK spontaneous mouse model by crossing *Pdgfb-iCre^ERT; Fak^fl/fl* where FAK deletion is under the control of tamoxifen inducible Cre, with the spontaneous PDAC model *Pdx1-flp; frt-STOP-frt-Kras^G12D/+; p53^frt/+* (KPF; ref. 18) where Kras activation and p53 deletion in the pancreas is induced by flippase (Flp) under the constitutive control of the mouse *Pdx1* promoter. Tamoxifen was administered to *Pdx1-flp; frt-STOP-frt-Kras^G12D/+;*
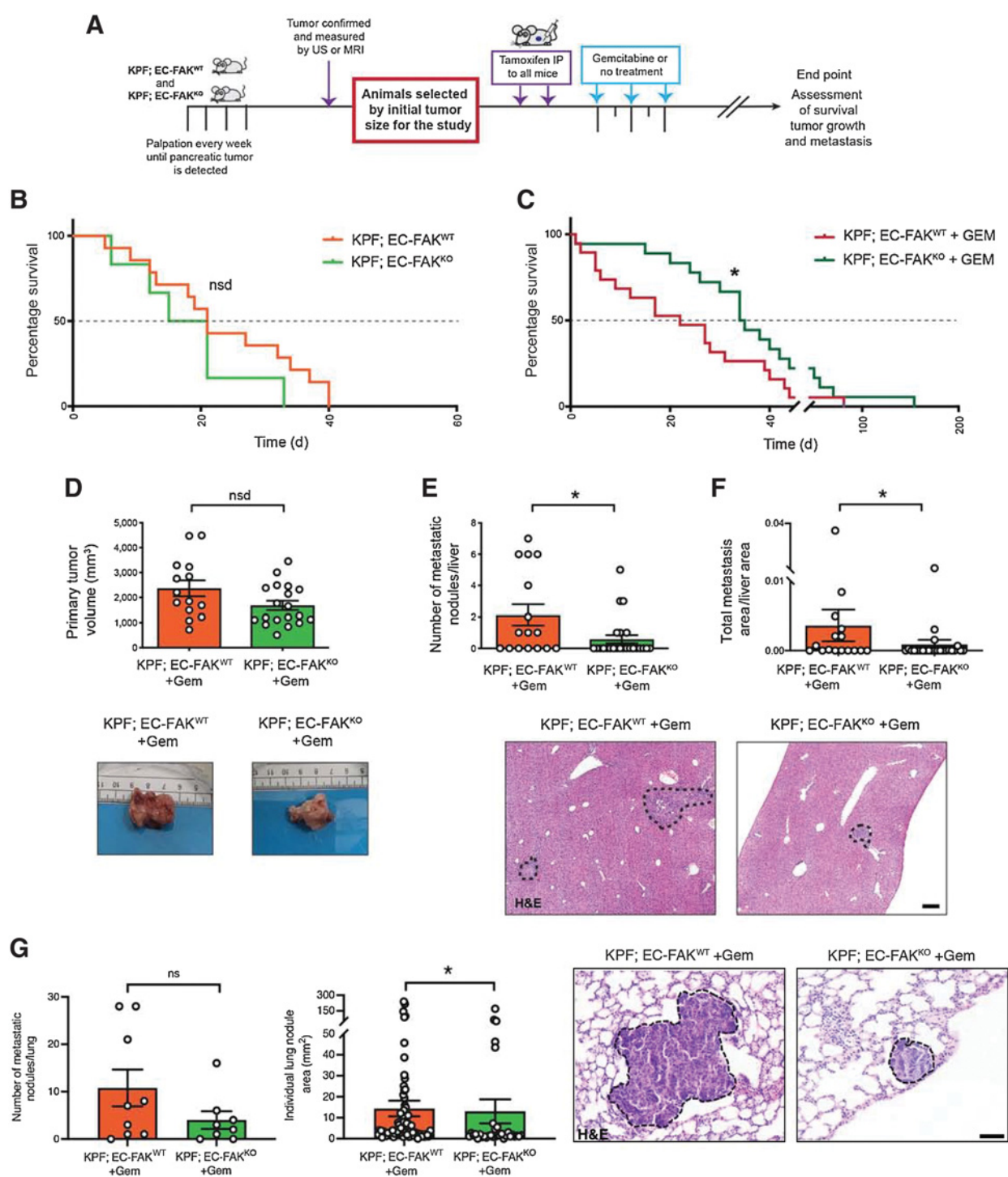
Figure 1.
EC-FAK deletion in mice with established 8661 pancreatic cancer cells does not affect primary tumor growth but reduces liver metastasis upon gemcitabine treatment. Pancreatic cancer cells were injected into the pancreas of both Cre$^+$ and Cre$^-$ Pdgfb-iCre^{ERT}; Fak$^{fl/fl}$ mice. Once the tumor was established, FAK deletion was induced by giving tamoxifen. Tumor growth, monitored by MRI (red dashed lines, tumor), after treatment with either saline (**A**) or gemcitabine (**B**). Saline treated, $n = 8$ WT and 13 KO mice; gemcitabine treated, $n = 15$ WT and 12 KO mice; values ± SEM. Representative MRI, gross tumor images (day 26), and H&E images are shown. Scale bar, 0.5 cm for gross tumor and H&E images. **C,** Tumor weight was not affected by gemcitabine treatment for either genotype. Saline treated, $n = 5$ WT and 4 KO; gemcitabine treated, $n = 8$ WT and 7 KO mice. Bar charts show mean values ± SEM. Mann–Whitney statistical test. **D,** Number of metastatic liver nodules in saline-treated (day 33–41, $n = 8$ WT and 7 KO mice) or gemcitabine-treated (day 44–51, $n = 15$ WT and 9 KO mice) mice, respectively. Pooled data from two independent experiments. **E,** Liver metastasis area is not affected in saline-treated EC-FAK^{WT} versus EC-FAK^{KO} mice; $n = 26$ WT nodules and 45 KO nodules. **F,** Liver metastasis area is reduced significantly in gemcitabine-treated EC-FAK^{KO} versus EC-FAK^{WT} mice ($n = 55$ KO and 148 WT nodules). Bar charts show mean values ± SEM; **, $P < 0.001$, Mann–Whitney statistical test. Representative pictures of H&E-stained livers with metastatic nodules are shown for both EC-FAK^{WT} and EC-FAK^{KO} saline treated. All H&E-stained section images were taken by Pannoramic scanner and viewed with 3D HISTECH software. White dashed lines, metastatic nodules. Scale bar, 200 μm. nsd, not statistically different.
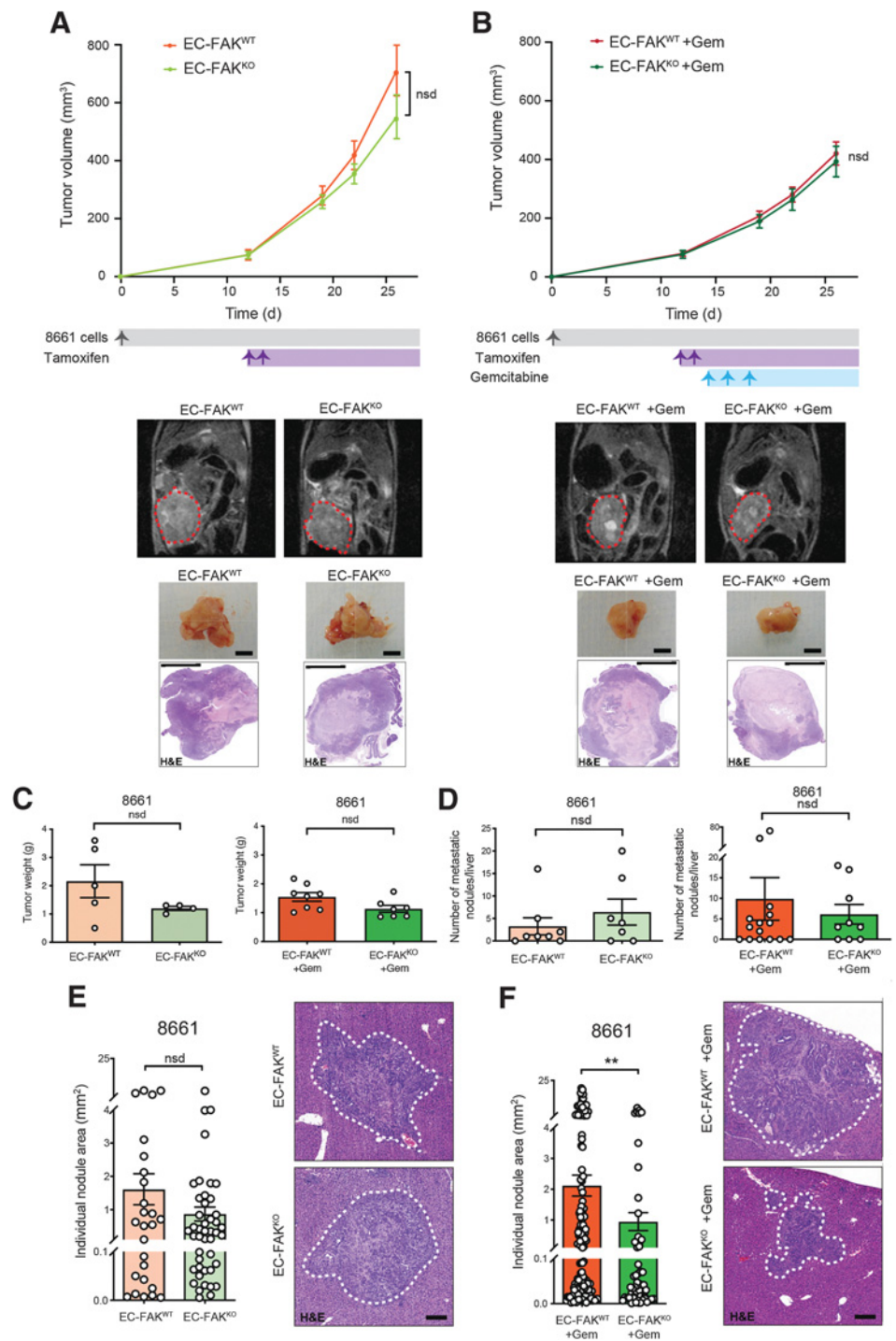
$p53^{frt/+}$; $Pdgfb$-$iCre^{ERT}$ +; $Fak^{fl/fl}$ and $Pdx1$-flp; frt-$STOP$-frt-$Kras^{G12D/+}$; $p53^{frt/+}$; $Pdgfb$-$iCre^{ERT}$ −; $Fak^{fl/fl}$ mice with palpable tumors to activate Pdgfb-driven iCre^{ERT} and induce *Fak* deletion and generate KPF; EC-FAK^{KO} and KPF; EC-FAK^{WT} mice, respectively. General histological H&E analysis of tissues from nontumor burdened KPF; EC-FAK^{WT} and KPF EC-FAK^{KO} mice showed no obvious differences in tissue morphology in pancreas, liver, kidney, heart, and lungs (Supplementary Fig. S4C), similar to the lack of any obvious defects in the organs of EC-FAK^{KO} mice described previously (12). Impor-

tantly, Western blot analysis identified that isolated lung ECs from KPF; EC-FAK^{KO} mice had a significant reduction in FAK expression when compared with ECs from KPF; EC-FAK^{WT} mice (Supplementary Fig. S4D). KPF; EC-FAK^{WT} and KPF; EC-FAK^{KO} mice showed no differences in primary tumor onset, body weight, Mendelian ratios or gender distribution (Supplementary Fig. S4E–S4H).

Tumor-burdened, tamoxifen-treated, KPF; EC-FAK^{WT} and KPF; EC-FAK^{KO} mice, were treated with gemcitabine, or saline as controls, and survival rates assessed (**Fig. 2A**). KPF; EC-FAK^{KO} mice showed

Figure 2.
EC-FAK deletion enhances the mean survival and decreases liver and lung metastasis of gemcitabine-treated but not untreated mice using the spontaneous *Pdx1-flp; frt-STOP-frt-Kras$^{G12D/+}$; p53$^{frt/+}$* (KPF) mice. **A,** KPF mice are a model of spontaneous PDAC. Schematic representation of experimental and treatment timeline for KPF; EC-FAK mice. **B,** Similar mean survival was observed between KPF; EC-FAK^{WT} and KPF; EC-FAK^{KO} mice; $n = 14$ WT and 6 KO mice. **C,** Gemcitabine-treated KPF; EC-FAK^{KO} mice had longer mean survival compared with gemcitabine-treated KPF; EC-FAK^{WT} control mice; $n = 19$ WT and 18 KO mice. Kaplan–Meier graphs. *, $P < 0.05$; Gehan–Breslow–Wilcoxon test. **D,** Tumor volume at endpoint between genotypes upon gemcitabine treatment; $n = 14$ WT and 19 KO mice; Mann–Whitney test. Representative images of gross tumors are shown for gemcitabine-treated KPF; EC-FAK^{WT} and KPF; EC-FAK^{KO} mice. **E** and **F,** Number of nodules (**E**) and metastatic burden (**F**) was calculated for gemcitabine-treated cohorts; $n = 16$ WT and 24 KO mice. **G,** Number of metastatic lung nodules ($n = 9$ WT and 8 KO mice) and individual nodule area for gemcitabine-treated mice was quantified ($n = 98$ WT and 33 KO lung nodules). *, $P < 0.05$ Mann–Whitney test. Representative images of H&E–stained liver and lung metastases are shown. All H&E-stained section images were taken by Pannoramic scanner and viewed with 3D HISTECH software. Black dashed lines, metastatic nodules. Scale bar in **F,** 200 μm; scale bar in **G,** 50 μm. All bar charts show mean values ± SEM. ns, nonsignificant; nsd, not statistically different.

efficient deletion of FAK in the tumor endothelium regardless of gemcitabine administration, as well as in the ECs of liver metastatic lesions (Supplementary Fig. S5A–S5D). In saline-treated KPF mice, loss of EC-FAK had no significant impact on survival (**Fig. 2B**). In contrast, gemcitabine-treated KPF; EC-FAK^{KO} mice had significantly longer survival time compared with gemcitabine treated KPF; EC-FAK^{WT} mice (**Fig. 2C**). In line with this, saline-treated KPF; EC-FAK^{WT} and KPF; EC-FAK^{KO} mice showed no differences in primary tumor growth (Supplementary Fig. S6A) or liver metastasis (Supplementary Fig. S6B–S6D). However, although gemcitabine-treated KPF; EC-FAK^{KO} and KPF; EC-FAK^{WT} mice had no significant differences in primary tumor volume (**Fig. 2D**), a significant decrease in the number of liver metastatic nodules and overall metastatic burden was observed in gemcitabine treated KPF; EC-FAK^{KO} mice compared with gemcitabine treated KPF; EC-FAK^{WT} mice (**Fig. 2E** and **F**). In addition, although the numbers of metastatic lung nodules was similar between KPF; EC-FAK^{WT} and KPF; EC-FAK^{KO}, individual lung nodule area was significantly reduced in KPF; EC-FAK^{KO} mice, upon gemcitabine treatment (**Fig. 2G**).

These data indicate that EC-FAK loss increases the median survival and decreases liver and lung metastasis of gemcitabine treated, but not saline-treated, KPF mice.

Loss of EC-FAK does not affect blood vessel density, leakage, or gemcitabine delivery in primary pancreatic tumors

Given that the tumor vasculature plays a key role in both tumor progression and metastatic dissemination and that EC-FAK has been described previously to affect tumor angiogenesis in other murine cancer models (12), we next asked whether loss of EC-FAK had an effect on tumor blood vessel density in the pancreatic 8661 orthotopic model upon gemcitabine treatment. Primary 8661 tumor sections were immunostained for endomucin and the blood vessel density was assessed by counting the number of blood vessels per unit area of viable tumor section. Primary tumor blood vessel density was not altered in gemcitabine-treated EC-FAK^{KO} compared with EC-FAK^{WT} mice (**Fig. 3A**). Tumor blood vessel leakage was assessed by measuring perivascular uptake of Hoechst dye injected via the tail vein in an antemortem process. No differences in Hoechst leakage were observed between gemcitabine treated EC-FAK^{WT} and EC-FAK^{KO} mice (**Fig. 3B**), suggesting no changes in tumor blood vessel leakage *in vivo*. To further examine the functionality of the blood vessels, we next tested the efficacy of gemcitabine (2′,2′-difluorodeoxycytidine, dFdC) delivery and metabolized gemcitabine dFdU (2′-deoxy-2′,2′-difluorouridine) in the primary tumor and nonmetastasized liver of EC-FAK^{WT} and EC-FAK^{KO} mice by LC-MS/MS. No differences in dFdC or dFdU levels were observed between genotypes in primary tumors or livers (**Fig. 3C** and **D**). These data indicate that EC-FAK loss does not affect primary tumor blood vessel density or leakage and has no apparent effect on gemcitabine delivery or metabolism, suggesting that the reduction in liver metastatic burden is not due to changes in these features.

EC-FAK regulates metastatic pancreatic tumor cell colonization in the liver of gemcitabine-treated mice, but does not affect numbers of circulating tumor cells, tumor cell homing or seeding

Metastatic burden can be affected by the intravasation of tumor cells from the primary tumor into the bloodstream to generate circulating tumor cells (CTC) followed by homing and seeding of tumor cells at a secondary site (33). 8661 tumor-burdened, gemcitabine-treated EC-FAK^{WT} and EC-FAK^{KO} mice showed no differences in numbers of

CTCs (CD45$^-$; Pdx1$^+$ population; (**Fig. 4A**; Supplementary Fig. S7A and S7B), suggesting that EC-FAK is not involved in the tumor cell escape from the primary tumor.

To assess tumor cell seeding, nontumor-bearing EC-FAK^{WT} and EC-FAK^{KO} mice were gemcitabine treated, intrasplenically injected with GFP-labeled 8661 cells and livers harvested and digested 2 hours after injection. Gemcitabine-treated EC-FAK^{WT} animals showed similar levels of GFP-positive cells in the liver compared with gemcitabine treated EC-FAK^{KO} mice (**Fig. 4B**; Supplementary Fig. S7C and S7D), indicating no changes in homing upon EC-FAK deletion and gemcitabine treatment.

To assess tumor cell seeding and colonization in the liver, EC-FAK^{WT} and EC-FAK^{KO} mice were gemcitabine treated, and sacrificed 48 hours and 7 days after tumor cell intrasplenic injection and the presence of pancreatic cancer–specific Pdx1-positive cells in the liver assessed. No statistical differences in percentage of animals with Pdx1-positive cells in the liver were observed at 48 hours between gemcitabine-treated EC-FAK^{WT} and EC-FAK^{KO} mice (**Fig. 4C**). However, at 7 days after 8661 intrasplenic injection, significantly fewer gemcitabine-treated EC-FAK^{KO} mice presented with tumor cells in the liver compared with gemcitabine-treated EC-FAK^{WT} control mice (**Fig. 4D**). In addition, the incidence of tumor cell colonies (counted as cell clusters with >3 cells) was also reduced in EC-FAK^{KO} gemcitabine-treated mice when compared with gemcitabine treated EC-FAK^{WT} mice (**Fig. 4E**). Together, these results indicate that EC-FAK deficiency combined with gemcitabine treatment does not affect numbers of CTCs, early pancreatic tumor cell homing or seeding but instead regulates the ability of tumor cells to successfully colonize in the liver.

### EC-FAK regulates phosphoproteomic signatures depending on oxygen availability

During the process of tumor cell establishment, the hepatic niche provides important angiocrine signals that influence the ability of metastasis-initiating cells to engraft and grow. High levels of hypoxia are a salient feature of primary PDAC (34) and can affect gemcitabine efficacy (35). Immunostaining for Glut1, a marker of tumor hypoxia, showed significantly increased levels of hypoxia in primary PDAC tumors compared with liver metastatic lesions in gemcitabine treated EC-FAK^{WT} mice (**Fig. 5A**). Given that ECs can activate distinct signaling pathways depending on the oxygen availability (36), we next asked whether EC-FAK regulated angiocrine responses to gemcitabine would be affected by exposure to hypoxia, thus possibly pointing toward differential effects observed in metastases but not in primary tumor growth.

We performed phosphoproteomic analysis of FAK-NULL (KO) ECs versus WT ECs from the following conditions: Hypoxia plus gemcitabine, normoxia minus gemcitabine or normoxia plus gemcitabine. EC FAK deficiency altered the number of phosphopeptides, detected by phosphoproteomics analysis when compared with WT ECs (**Fig. 5B**; Supplementary Fig. S8A–S8C). Further analysis identified significantly enriched regulatory phosphorylation sites (29) in FAK-NULL ECs versus WT ECs only in normoxia plus gemcitabine treatment conditions but not significant in the other conditions (**Fig. 5C**). Among them, Jun (Transcription factor AP-1) and Mapk7 phospho-sites were found to be enriched in FAK-KO ECs in normoxic conditions plus gemcitabine versus WT ECs under the same conditions. In contrast, Map2Ks (Dual specificity MAPKs), Akt (RAC-alpha serine/threonine- protein kinase), Raf1 (RAF proto-oncogene serine/threonine-protein kinase), and Pak1 (serine/threonine–protein kinase) were downregulated in normoxia plus gemcitabine FAK-KO
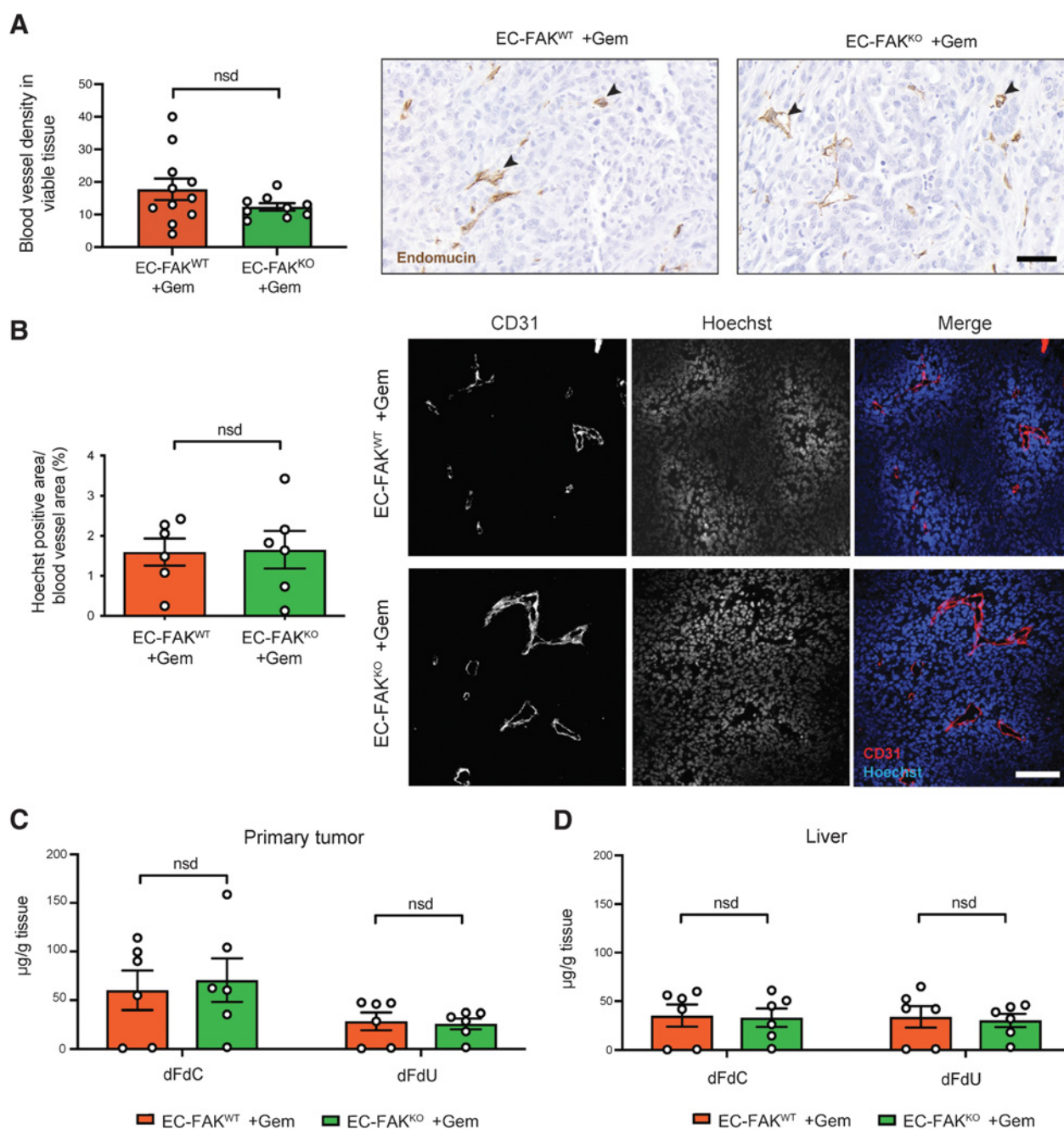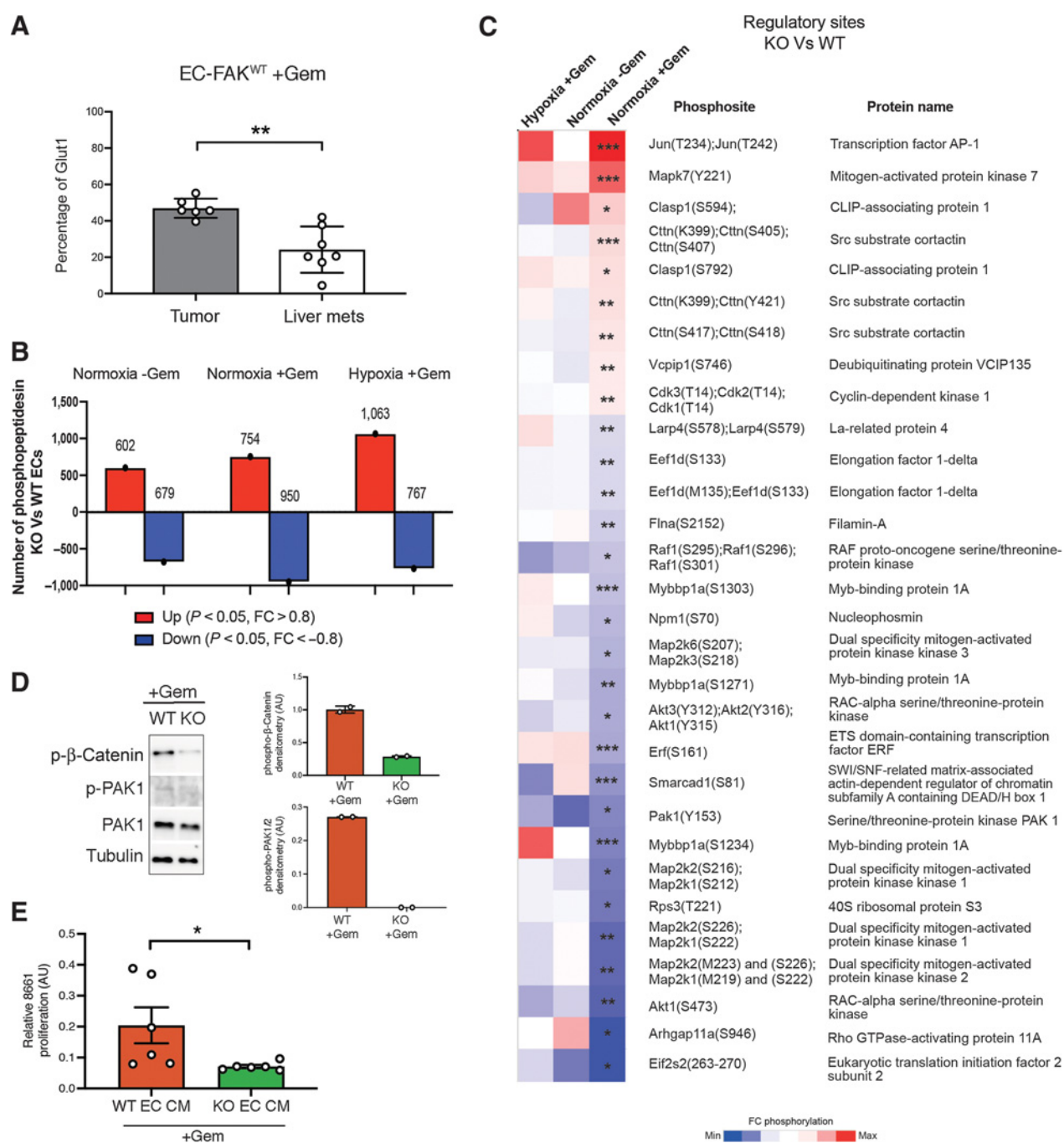
Figure 3.
Loss of EC-FAK does not affect blood vessel density or leakage in the primary tumor or gemcitabine delivery. **A,** Primary tumor blood vessel density, number of endomucin +ve blood vessels per live tumor area, of gemcitabine-treated EC-FAK^{WT} and EC-FAK^{KO} mice; $n = 11$ WT and 9 KO mice. Representative images of endomucin-immunostained tumor blood vessels shown were taken by Panoramic scanner and viewed with 3D HISTECH software. Scale bar, 50 μm. Arrowheads, representative blood vessels. **B,** Vessel leakage is unchanged between gemcitabine-treated EC-FAK^{WT} and EC-FAK^{KO} mice. Tumor-bearing mice were injected via the tail vein with Hoechst dye in an antemortem process to assess blood vessel leakage. Tumor sections were stained for CD31 and analyzed for area of Hoechst uptake in tumor cells per CD31-positive blood vessel area. $n = 6$ mice per experimental group. Representative images of tumor sections showing Hoechst and CD31 staining. Scale bar, 100 μm. **C** and **D,** Gemcitabine delivery is not altered by loss of EC-FAK. At day 28, tumor-bearing mice were injected with a high dose of gemcitabine intraperitoneally in an antemortem process and delivery of unprocessed or metabolized gemcitabine (dFdC and dFdU) was assessed in the primary tumor (**C**) and liver (**D**) by LC-MS/MS. Bar charts show mean values ± SEM. Mann–Whitney test; $n = 6$ mice per the experimental group. nsd, not statistically different.
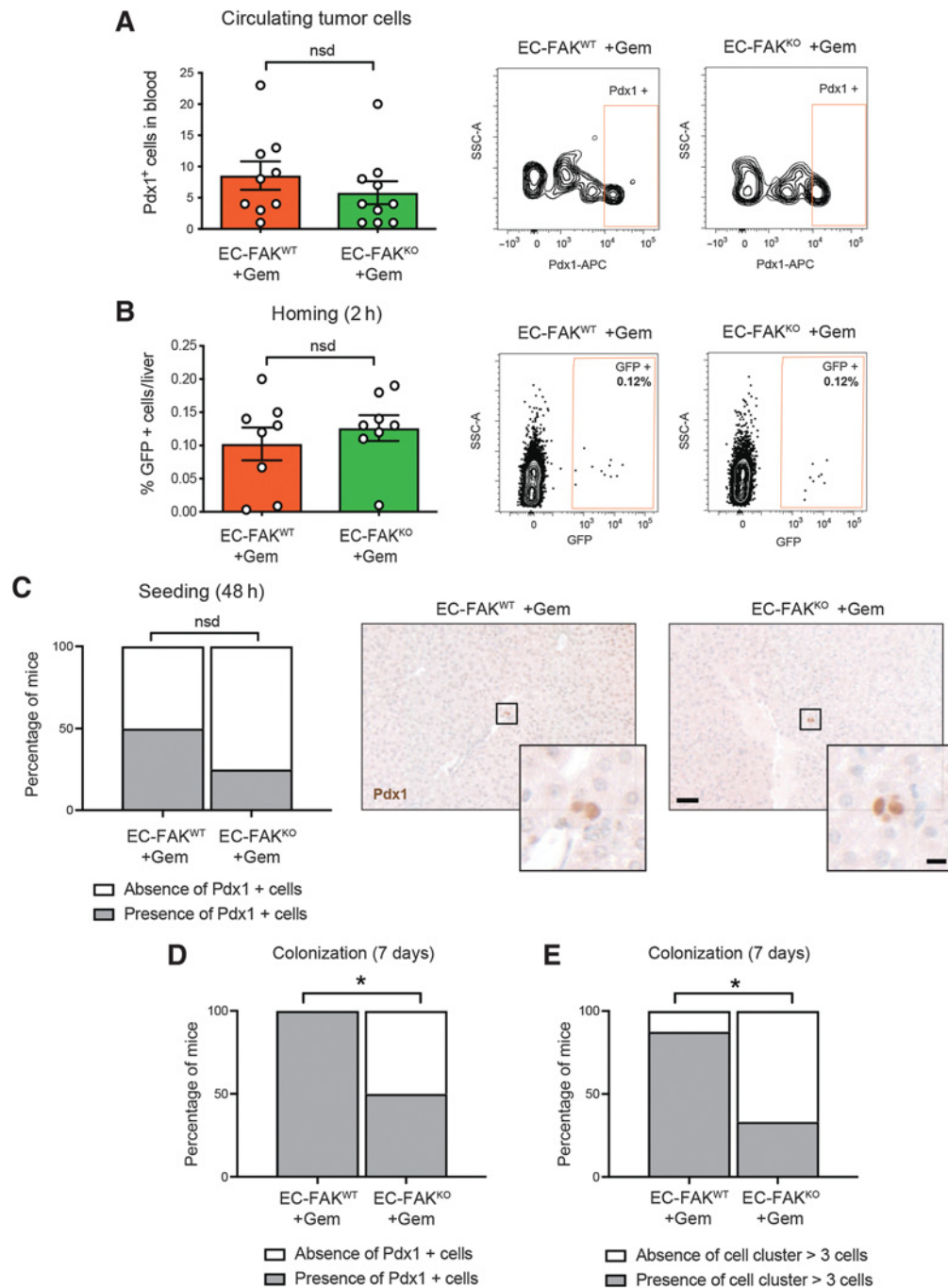
Figure 4.
EC-FAK deletion in gemcitabine-treated mice does not affect numbers of circulating tumor cells or tumor cell homing/seeding to the liver but reduces liver metastasis colonization. **A,** Numbers of circulating tumor cells are not affected by EC-FAK loss in gemcitabine-treated mice. 8661 cancer cells were injected into the pancreas of both *Pdgfb-iCre*[ERT] +; *Fak*^{fl/fl} (EC-FAKKO) and *Pdgfb-iCre*[ERT−]; *Fak*^{fl/fl} (EC-FAKWT) mice and given tamoxifen to induce EC-FAK deletion in Cre^{+} mice. All mice were treated with gemcitabine. At day 41 after 8661 tumor cell inoculation, flow cytometry of CD45^{−}/Pdx1^{+} cells isolated from the blood were considered circulating tumor cells. $n = 9$ WT and 10 KO mice; Mann–Whitney test. **B,** Tumor cell homing. EC-FAK[WT] and EC-FAK[KO] mice were treated with gemcitabine before performing intrasplenic injection of GFP-labeled 8661 pancreatic cancer cells. Two hours after tumor cell injection the percentage of GFP^{+} tumor cells seeding in the liver was assessed. $n = 8$ mice per group; Mann–Whitney test. **C,** Tumor cell seeding. Intrasplenic injections of 8661 cells was performed as in **B** and livers harvested at 48 hours after injection. Immunostaining of Pdx1 was performed and Pdx1-positive cells were identified as metastatic cancer cells in the liver. The same number of mice presented with Pdx1 + cells after 48 hours ($n = 8$ mice per genotype). Representative images of Pdx1 staining in the liver shown for both experimental groups at 48 hours after injection were taken by Pannoramic scanner and viewed with 3D HISTECH software. Scale bar, 50 μm. Higher power insets, 10 μm. **D,** Tumor cell colonization in the liver is reduced in gemcitabine-treated EC-FAK[KO] mice. At 7 days after intrasplenic injection of 8661 cells, EC-FAK loss combined with gemcitabine treatment caused a decrease in the percentage of animals with Pdx1 + cells in the liver (**E**) and with cell clusters of more than 3 cancer cells. $n = 8$ WT and 6 KO mice. All bar charts show mean values ± SEM. *, $P < 0.05$ χ^2 test applied in incidence data. nsd, not statistically different.

Figure 5.
EC-FAK regulates different signaling pathways upon gemcitabine treatment under hypoxic or normoxic conditions. **A,** The percentage of hypoxic area, assessed by Glut-1–positive area, is enhanced in primary pancreatic tumors compared with liver metastases of gemcitabine-treated EC-FAK[WT] mice; $n = 6$ tumor and 7 metastases; ∗∗, $P < 0.01$; Mann–Whitney test. Bar charts show mean values $\pm$ SEM. **B,** Phosphoproteomics analyses were performed using FAK-NULL ECs (KO) versus WT ECs in hypoxia plus gemcitabine, normoxia minus gemcitabine, or normoxia plus gemcitabine conditions. Number of phosphopeptides significantly up/downregulated ($P < 0.05$ and $> \pm 0.8$ fold change) in FAK-NULL ECs versus WT ECs for each condition. **C,** Heatmap of regulatory phosphosites significantly enriched in FAK-NULL ECs versus WT ECs in normoxic conditions plus gemcitabine (Gem), but not in the other conditions. ∗, $P < 0.05$; ∗∗, $P < 0.01$; ∗∗∗, $P < 0.001$. $n = 3$ samples per condition. **D,** Phospho-PAK1 and phospho–β-catenin protein levels are significantly reduced in FAK-NULL ECs compared with WT ECs. Bar charts show mean $\pm$ SD for phospho–β-catenin and phospho-PAK densitometry (AU); $n = 2$ cell preps per condition. Tubulin is the loading control. **E,** Conditioned medium (CM) from gemcitabine-treated FAK-NULL ECs significantly reduced tumor cell proliferation versus gemcitabine-treated WT ECs. ∗, $P < 0.05$; ∗∗∗∗, $P < 0.0001$; $n = 2$ cell preps per condition. Bar charts show mean values $\pm$ SEM.

ECs versus WT ECs. We examined phosphorylated PAK1 levels in FAK-KO and WT ECs, both in the presence of gemcitabine, and showed that FAK loss in ECs downregulates signaling through phospho-PAK1 and, downstream of PAK1, β-catenin (37), suggesting an association of inhibition of the PAK1–β-catenin signaling pathway in FAK-KO ECs (**Fig. 5D**). Medium from these cells (CM) was added to 8661 tumor cells for up to 72 hours, to mimic the metastatic environment (i.e., in normoxia) and tumor cell proliferation was measured. CM from gemcitabine-treated FAK-KO ECs significantly reduced tumor cell proliferation (**Fig. 5E**). These results suggest that EC can control tumor growth via angiocrine signals regulated by a combination of FAK and gemcitabine.

These results indicate that loss of FAK affects phosphoproteomic profiles in ECs depending on oxygen availability and gemcitabine treatment. Overall, our data suggest that angiocrine signals from ECs can regulate tumor cell proliferation at the secondary site to mediate metastasis. Deletion of EC-FAK inhibits these signals to reduce metastatic growth.

Low EC-FAK expression correlates with better survival and reduced relapse incidence in gemcitabine-treated patients with PDAC

Given that metastatic dissemination is a defining indicator of poor prognosis among patients with PDAC, we explored whether endothelial FAK expression levels could have clinical relevance in correlating with patient survival after gemcitabine treatment. EC-FAK expression was examined by immunofluorescence in primary PDAC tumor sections from patients treated with gemcitabine alone or in combination with other treatments and the percentage of EC-FAK–negative blood vessels across individual patients was calculated. This revealed a mean of 44% of blood vessels being EC-FAK–negative across individual patients (**Fig. 6A** and **B**). Patients with a high number of EC-FAK–negative vessels had significantly improved survival and decreased incidence of relapse compared with patients with a low number of EC-FAK–negative vessels (**Fig. 6C** and **D**). These results provide clinically relevant evidence to support the notion that low levels of EC-FAK in the primary tumor vasculature improves survival of gemcitabine-treated human patients with PDAC.

Discussion

PDAC is a highly aggressive disease associated with a very poor outcome. Gemcitabine is part of the first-line treatment given to patients with advanced metastatic disease. For many of the less advanced disease patients, where primary resection is possible, distant metastasis ensues. Thus, understanding the mechanisms that enable the control of metastatic growth becomes an important goal (38).

Here, we have identified a new role for EC-FAK in regulating metastasis upon gemcitabine treatment that has effects on survival, both in murine models and human patients. Our results show no changes in primary pancreatic tumor growth upon EC-FAK loss (Supplementary Fig. S8D). Previous studies performed using the *Pdgfb-iCre*^ERT^; *Fak*^fl/fl^ mouse model have shown differences in tumor growth when deleting EC-FAK before tumor formation (12). However, no differences were shown when EC-FAK was deleted after the tumor was established (15, 17) and our results corroborate these findings. Other studies using the EC-FAK heterozygous K454R mutant-KD mouse model also reported no differences on tumor growth, further confirming our results (13). Interestingly, EC-FAK mutated at Y397 or Y861 residues has differential effects on tumor growth and tumor angiogenesis (14), indicating that

beyond its kinase activity, the phosphorylated sites are also important for the regulation of tumor angiogenesis and subsequent tumor growth.

EC-FAK loss combined with chemotherapy can have different effects depending on the chemotherapeutic agent and type of cancer. In contrast to no differences in pancreatic tumor growth of gemcitabine treated EC-FAK–deleted mice shown here, doxorubicin-treated EC-FAK–deleted mice showed reduced melanoma tumor growth (17). Similar to EC-FAK–deleted doxorubicin-treated mice (17), tumor angiogenesis of EC-FAK–deleted gemcitabine–treated mice was not affected, despite the pro-angiogenic effect of gemcitabine previously described (39).

Our results indicate differences in metastasis in EC-FAK–deleted, gemcitabine-treated mice. Multiple studies have demonstrated a role for FAK in regulating vascular integrity and barrier function in a physiological context (40, 41) and in cancer (12, 13, 17, 42). A previous study reported that EC-FAK kinase activity can impact on the metastatic process by regulating VEGF-stimulated vascular permeability through phosphorylation of VEC-Y658. Although no confirmation of vascular leakage was shown *in vivo*, the authors suggest that the difference in metastasis is due to changes in EC-permeability regulated by EC-FAK in breast cancer (13). This permeability phenotype, correlated with VEC-Y658 phosphorylation, was corroborated by another study using the same EC-FAK KD mouse model (42). In contrast, our results do not show differences in blood vessel leakage and instead, recapitulate results previously shown in this regard with the same EC-FAK^KO mouse model (17). Given that most of the reports studied EC-FAK in response to VEGF, the differences in vascular leakage may rely on the characteristics of the tumor. Although ovarian and melanoma tumors are highly vascularized with elevated VEGFA expression (43), pancreatic tumors are poorly vascularized and most likely have lower amounts of VEGF. In contrast to Jean and colleagues (13), in the present study, differences in metastasis regulated by EC-FAK were observed only upon gemcitabine treatment. No differences in vascular leakage and CTCs upon EC-FAK loss and gemcitabine treatment were observed, suggesting that EC-FAK is not regulating metastasis by affecting the escape of tumor cells from the primary pancreatic adenocarcinoma.

Previously published studies have revealed that metastatic target organs are modified before the arrival of disseminating tumor cells by primary tumor-secreted factors creating a pre-metastatic niche (44). For example, PDAC-derived exosomes induce liver pre-metastatic niche formation by regulating a fibrotic reaction that enhances bone-marrow derived macrophage recruitment into the liver (45). Interestingly, liver ECs can also regulate hepatic metastasis in an angiocrine independent manner (46). In addition, hepatocytes have recently been described to influence the formation of the pre-metastatic niche in the liver by inducing fibrosis and accumulation of myeloid cells (47) and sc-RNAseq of liver ECs and hepatocytes has shown zonated vascular signaling mechanisms that may be involved in responses to cancer (48). Our data, using the intrasplenic model, show differences in liver colonization upon EC-FAK deletion and gemcitabine treatment in the absence of a primary tumor, suggesting that changes in the hepatic vasculature are enough to modulate metastatic engraftment. Our results indicate that tumor cells are less able to colonize in gemcitabine-treated EC-FAK–depleted livers after 7 days after injection. Interestingly, EC-FAK has been previously described to modulate metastasis in the lungs (13) and correlates with our findings that lung metastasis area is reduced significantly in EC-FAKKO mice treated with gemcitabine at least in the TB32048 and KPF models. Notably, this study showed no differences in initial cell homing and adhesion
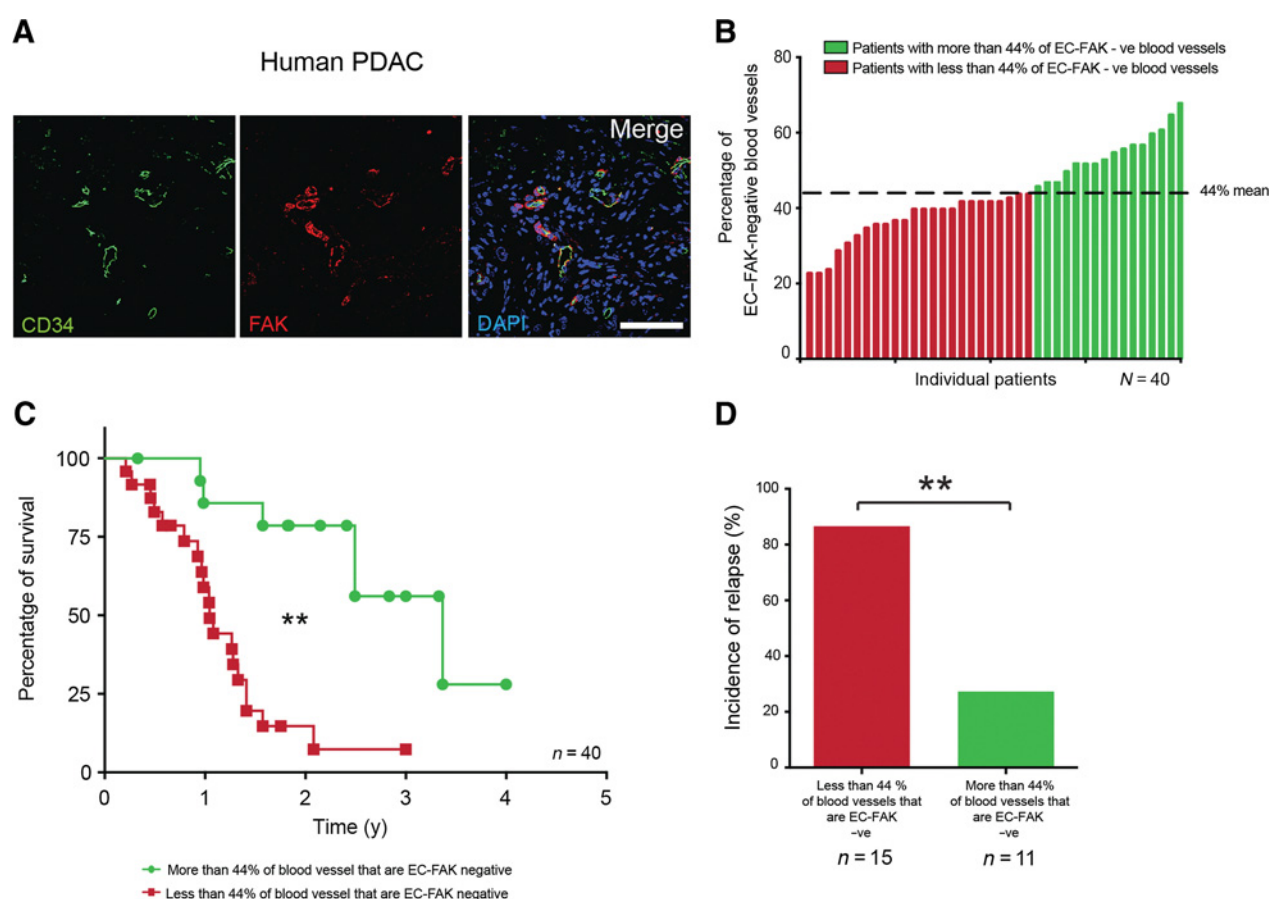
Figure 6.
Low EC-FAK expression correlates with improved survival and less incidence of relapse in human pancreatic gemcitabine-treated patients. **A,** Human pancreatic ductal adenocarcinoma biopsies ($n = 40$ individual patient samples) were double immunostained for FAK and the EC marker CD34. Representative images of double immunostained sections are given. Scale bar, 50 μm. **B,** Quantitation of the percentage of EC-FAK–negative blood vessels across individual patients revealed that 16 out of 40 patients (green bars) have more than the mean (44) percentage of EC-FAK–negative vessels. **C,** Kaplan–Meier curves. Patients with more than the mean percentage of EC-FAK–negative vessels have significantly improved survival compared with patients with less than the mean percentage of EC-FAK–negative vessels. Log-rank statistical test. **D,** Patients with more than the mean percentage of EC-FAK–negative vessels have significantly decreased incidence of relapse ($n = 26$ patients). Fisher exact test applied; **, $P < 0.01$.

(6 hours) but showed fewer cells engrafted in the lungs at 16 hours upon EC-FAK inhibition. These observations are in line with our findings as no differences were observed in homing or seeding but less colonization was found upon EC-FAK deletion with gemcitabine treatment. In fact, EC-FAK has been described previously to modulate cancer cell homing in the lungs by upregulating E-selectin (49).

Liver metastases are significantly less hypoxic than primary tumors, and both cancer cells and ECs can trigger different signaling pathways in different oxygen conditions (36). Also, hypoxia has been shown to affect EC angiocrine signals (50). Therefore, we hypothesize that different environmental hypoxia levels could explain a different angiocrine regulation by EC-FAK causing a reduction of metastatic growth without influencing primary tumor size. In fact, phosphoproteomic analysis revealed that gemcitabine-treated FAK-KO ECs downregulate the MAP kinase cascade in normoxic conditions (which resemble the liver metastatic site) and not in hypoxic conditions (more similar to the primary tumor). MAPK signaling pathway has been largely studied due to its

multiple functions regulating cancer progression (51), including the modulation of cell survival and apoptosis (52). Our data also show significant downregulation of RAF proto-oncogene serine/threonine protein kinase (Raf1) and Filamin-A (FlnA) in ECs upon FAK deletion and gemcitabine treatment only in normoxic conditions. Raf1 can activate the MAPK pathway as well as promote cell survival by antagonizing apoptosis (53) and KO of FlnA in ECs has been shown to reduce fibrosarcoma growth (54). Moreover, overexpression of some MAP3K can lead to the activation of p38 and JNK pathways (55). The p38 pathway in ECs has been described previously as a major regulator or tumor progression and metastasis (56). Other p38 activators are the p21-activated kinases (PAK). In the present study, phosphorylation of the serine/threonine–protein kinase PAK 1 (PAK1) was significantly reduced in ECs upon FAK deletion and gemcitabine treatment in normoxia but to a lesser extent in hypoxia conditions. PAK1 is a protein kinase that plays an essential role downstream of receptor-type kinases and integrins in several signaling pathways regulating actin cytoskeleton dynamics, cell polarity, invasion, and apoptosis

among others (57). In fact, PAK1 inhibition has been shown to increase effector caspase activation and apoptosis in non–small cell lung cancer cells (58) and to phosphorylate death agonist Bad to protect cells from apoptosis (59). Notably, some studies show that PAK1 inhibitors reduce pancreatic cancer cell growth *in vivo* (60) and improve gemcitabine efficacy in murine pancreatic cancer models (61). Furthermore, PAK1 regulates β-catenin activation and overexpression of PAK1 is correlated with accumulation of β-catenin in colon cancer to drive cancer progression (37). These molecular changes observed in gemcitabine treated ECs regulated by FAK are possibly part of an angiocrine signal that may regulate tumor cell survival and apoptosis in the metastatic secondary site. Indeed, our results show that CM from gemcitabine-treated FAK-NULL ECs was able to significantly reduce tumor cell proliferation. One possibility is that changes in the PAK–β-catenin signaling pathway may drive changes in angiocrine production when FAK is deleted in ECs, to regulate metastatic tumor growth. Why this is not seen in the primary tumor could be explained by differences in the expression of genes in ECs from different tissue beds (62) differentially regulating tumor cell growth or by the difference in levels of hypoxia between the primary and metastatic tumor environment.

Most importantly, our data revealed that the reduction of liver metastasis regulated by EC-FAK was enough to improve survival rates in our gemcitabine treated KPF spontaneous mouse model. Moreover, gemcitabine-treated patients with low levels of EC-FAK showed a better survival rate and were less prone to relapse, confirming the clinical relevance of these findings.

Data indicating FAK as an effective therapeutic target has led to the development of FAK inhibitors (63). Some studies have already shown the benefits of FAK inhibitors alone or in combination with other therapies (64). FAK is hyperactivated in PDAC where it is implicated in increased fibrosis and inflammation and is associated with poor prognosis. FAK inhibitors have been shown *in vitro* and *in vivo* to inhibit tumor growth and metastasis (65), and in combination with other chemotherapeutics can potentiate efficacy. Our findings further corroborate this idea by showing a direct positive effect of low FAK expression in the EC compartment on survival of gemcitabine-treated patients.

Overall, our results show a novel role of EC-FAK in PDAC when combined with gemcitabine treatment highlighting the importance of the tumor vasculature regulating the efficacy of chemotherapy. EC-FAK in the presence of gemcitabine regulates liver metastasis directly affecting survival in both mouse models and patients. These findings open new avenues for considering the potential utility of the combination of FAK inhibitors with gemcitabine in future clinical applications, leading to new ways of controlling liver metastasis in patients with PDAC.

Authors' Disclosures

Authors' Contributions

M. Roy-Luzarraga: Conceptualization, data curation, formal analysis, validation, investigation, visualization, methodology, writing–original draft, writing–review and editing. **L.E. Reynolds:** Supervision, investigation, writing–review and editing. **B. de Luxán-Delgado:** Formal analysis, validation, investigation, writing–review and editing. **O. Maiques:** Software, investigation, methodology, writing–review and editing. **L. Wisniewski:** Validation, investigation, writing–review and editing. **E. Newport:** Investigation. **V. Rajeeve:** Formal analysis, methodology. **R.J.G. Drake:** Investigation. **J. Gómez-Escudero:** Formal analysis, visualization. **F.M. Richards:** Validation, investigation, writing–review and editing. **C. Weller:** Validation, investigation. **C. Dormann:** Validation, investigation. **Y. Meng:** Validation, investigation. **P.B. Vermeulen:** Formal analysis, supervision, writing–review and editing. **D. Saur:** Resources, writing–review and editing. **V. Sanz-Moreno:** Supervision, writing–review and editing. **P.P. Wong:** Resources, investigation, writing–review and editing. **C. Géraud:** Supervision, visualization, writing–review and editing. **P.R. Cutillas:** Formal analysis, supervision, writing–review and editing. **K. Hodivala-Dilke:** Conceptualization, resources, data curation, supervision, funding acquisition, visualization, writing–original draft, writing–review and editing.

Acknowledgments

References

1. Rawla P, Sunkara T, Gaduputi V. Epidemiology of pancreatic cancer: global trends, etiology and risk factors. World J Oncol 2019;10:10–27.
2. Andersson R, Aho U, Nilsson BI, Peters GJ, Pastor-Anglada M, Rasch W, et al. Gemcitabine chemoresistance in pancreatic cancer: molecular mechanisms and potential solutions. Scand J Gastroenterol 2009;44:782–6.
3. Sun Y, Campisi J, Higano C, Beer TM, Porter P, Coleman I, et al. Treatment-induced damage to the tumor microenvironment promotes prostate cancer therapy resistance through WNT16B. Nat Med 2012;18:1359–68.
4. Acharyya S, Oskarsson T, Vanharanta S, Malladi S, Kim J, Morris PG, et al. A CXCL1 paracrine network links cancer chemoresistance and metastasis. Cell 2012;150:165–78.
5. Cao Z, Scandura JM, Inghirami GG, Shido K, Ding BS, Rafii S. Molecular checkpoint decisions made by subverted vascular niche transform indolent tumor cells into chemoresistant cancer stem cells. Cancer Cell 2017;31:110–26.
6. Wieland E, Rodriguez-Vita J, Liebler SS, Mogler C, Moll I, Herberich SE, et al. Endothelial Notch1 activity facilitates metastasis. Cancer Cell 2017;31:355–67.
7. Lu J, Ye X, Fan F, Xia L, Bhattacharya R, Bellister S, et al. Endothelial cells promote the colorectal cancer stem cell phenotype through a soluble form of Jagged-1. Cancer Cell 2013;23:171–85.
8. Zhang Z, Dong Z, Lauxen IS, Filho MS, Nor JE. Endothelial cell-secreted EGF induces epithelial-to-mesenchymal transition and endows head and neck cancer cells with stem-like phenotype. Cancer Res 2014;74:2869–81.
9. Cao Z, Ding BS, Guo P, Lee SB, Butler JM, Casey SC, et al. Angiocrine factors deployed by tumor vascular niche induce B-cell lymphoma invasiveness and chemoresistance. Cancer Cell 2014;25:350–65.
10. Gilbert LA, Hemann MT. DNA damage-mediated induction of a chemoresistant niche. Cell 2010;143:355–66.
11. Sulzmaier FJ, Jean C, Schlaepfer DD. FAK in cancer: mechanistic findings and clinical applications. Nat Rev Cancer 2014;14:598–610.
12. Tavora B, Batista S, Reynolds LE, Jadeja S, Robinson S, Kostourou V, et al. Endothelial FAK is required for tumour angiogenesis. EMBO Mol Med 2010;2:516–28.
13. Jean C, Chen XL, Nam JO, Tancioni I, Uryu S, Lawson C, et al. Inhibition of endothelial FAK activity prevents tumor metastasis by enhancing barrier function. J Cell Biol 2014;204:247–63.
14. Pedrosa AR, Bodrug N, Gomez-Escudero J, Carter EP, Reynolds LE, Georgiou PN, et al. Tumor angiogenesis is differentially regulated by phosphorylation of endothelial cell focal adhesion kinase tyrosines-397 and -861. Cancer Res 2019;79:4371–86.
15. Newport E, Pedrosa AR, Lees D, Dukinfield M, Carter E, Gomez-Escudero J, et al. Elucidating the role of the kinase activity of endothelial cell focal adhesion kinase in angiocrine signalling and tumour growth. J Pathol 2022;256:235–47.
16. Roy-Luzarraga M, Hodivala-Dilke K. Molecular pathways: endothelial cell FAK-a target for cancer treatment. Clin Cancer Res 2016;22:3718-24.
17. Tavora B, Reynolds LE, Batista S, Demircioglu F, Fernandez I, Lechertier T, et al. Endothelial-cell FAK targeting sensitizes tumours to DNA-damaging therapy. Nature 2014;514:112–6.
18. Schonhuber N, Seidler B, Schuck K, Veltkamp C, Schachtler C, Zukowska M, et al. A next-generation dual-recombinase system for time- and host-specific targeting of pancreatic cancer. Nat Med 2014;20:1340–7.
19. von Burstin J, Eser S, Paul MC, Seidler B, Brandl M, Messer M, et al. E-cadherin regulates metastasis of pancreatic cancer in vivo and is suppressed by a SNAIL/HDAC1/HDAC2 repressor complex. Gastroenterology 2009;137:361–71.
20. Falcomata C, Barthel S, Widholz SA, Schneeweis C, Montero JJ, Toska A, et al. Selective multi-kinase inhibition sensitizes mesenchymal pancreatic cancer to immune checkpoint blockade by remodeling the tumor microenvironment. Nat Cancer 2022;3:318–36.
21. Bapiro TE, Frese KK, Courtin A, Bramhall JL, Madhu B, Cook N, et al. Gemcitabine diphosphate choline is a major metabolite linked to the Kennedy pathway in pancreatic cancer models in vivo. Br J Cancer 2014;111:318–25.
22. Orgaz JL, Crosas-Molist E, Sadok A, Perdrix-Rosell A, Maiques O, Rodriguez-Hernandez I, et al. Myosin II reactivation and cytoskeletal remodeling as a hallmark and a vulnerability in melanoma therapy resistance. Cancer Cell 2020;37:85–103.
23. Reynolds LE, Hodivala-Dilke KM. Primary mouse endothelial cell culture for assays of angiogenesis. Methods Mol Med 2006;120:503–9.
24. Hijazi M, Smith R, Rajeeve V, Bessant C, Cutillas PR. Reconstructing kinase network topologies from phosphoproteomics data reveals cancer-associated rewiring. Nat Biotechnol 2020;38:493–502.
25. Wilkes EH, Terfve C, Gribben JG, Saez-Rodriguez J, Cutillas PR. Empirical inference of circuitry and plasticity in a kinase signaling network. Proc Natl Acad Sci U S A 2015;112:7719–24.
26. Cutillas PR. Targeted in-depth quantification of signaling using label-free mass spectrometry. Methods Enzymol 2017;585:245–68.
27. Casado P, Rodriguez-Prados JC, Cosulich SC, Guichard S, Vanhaesebroeck B, Joel S, et al. Kinase-substrate enrichment analysis provides insights into the heterogeneity of signaling pathway activation in leukemia cells. Sci Signal 2013;6:rs6.
28. Dinkel H, Chica C, Via A, Gould CM, Jensen LJ, Gibson TJ, et al. Phospho.ELM: a database of phosphorylation sites—update 2011. Nucleic Acids Res 2011;39:D261–7.
29. Hornbeck PV, Zhang B, Murray B, Kornhauser JM, Latham V, Skrzypek E. PhosphoSitePlus, 2014: mutations, PTMs, and recalibrations. Nucleic Acids Res 2015;43:D512–20.
30. Wong PP, Demircioglu F, Ghazaly E, Alrawashdeh W, Stratford MR, Scudamore CL, et al. Dual-action combination therapy enhances angiogenesis while reducing tumor growth and spread. Cancer Cell 2015;27:123–37.
31. Perez-Riverol Y, Csordas A, Bai J, Bernal-Llinares M, Hewapathirana S, Kundu DJ, et al. The PRIDE database and related tools and resources in 2019: improving support for quantification data. Nucleic Acids Res 2019;47:D442–D50.
32. Mehta KJ, Farnaud SJ, Sharp PA. Iron and liver fibrosis: mechanistic and clinical aspects. World J Gastroenterol 2019;25:521–38.
33. Valastyan S, Weinberg RA. Tumor metastasis: molecular insights and evolving paradigms. Cell 2011;147:275–92.
34. Petrova V, Annicchiarico-Petruzzelli M, Melino G, Amelio I. The hypoxic tumour microenvironment. Oncogenesis 2018;7:10.
35. Yokoi K, Fidler IJ. Hypoxia increases resistance of human pancreatic cancer cells to apoptosis induced by gemcitabine. Clin Cancer Res 2004;10:2299–306.
36. Muz B, de la Puente P, Azab F, Azab AK. The role of hypoxia in cancer progression, angiogenesis, metastasis, and resistance to therapy. Hypoxia 2015;3:83–92.
37. Zhu G, Wang Y, Huang B, Liang J, Ding Y, Xu A, et al. A Rac1/PAK1 cascade controls beta-catenin activation in colon cancer cells. Oncogene 2012;31:1001–12.
38. Labori KJ, Katz MH, Tzeng CW, Bjornbeth BA, Cvancarova M, Edwin B, et al. Impact of early disease progression and surgical complications on adjuvant chemotherapy completion rates and survival in patients undergoing the surgery first approach for resectable pancreatic ductal adenocarcinoma—a population-based cohort study. Acta Oncol 2016;55:265–77.
39. Khan MA, Srivastava SK, Bhardwaj A, Singh S, Arora S, Zubair H, et al. Gemcitabine triggers angiogenesis-promoting molecular signals in pancreatic cancer cells: therapeutic implications. Oncotarget 2015;6:39140–50.
40. Chen XL, Nam JO, Jean C, Lawson C, Walsh CT, Goka E, et al. VEGF-induced vascular permeability is mediated by FAK. Dev Cell 2012;22:146–57.
41. Schmidt TT, Tauseef M, Yue L, Bonini MG, Gothert J, Shen TL, et al. Conditional deletion of FAK in mice endothelium disrupts lung vascular barrier function due to destabilization of RhoA and Rac1 activities. Am J Physiol Lung Cell Mol Physiol 2013;305:L291–300.
42. Alexopoulou AN, Lees DM, Bodrug N, Lechertier T, Fernandez I, D'Amico G, et al. Focal Adhesion Kinase (FAK) tyrosine 397E mutation restores the vascular leakage defect in endothelium-specific FAK-kinase dead mice. J Pathol 2017;242:358–70.
43. Masoumi Moghaddam S, Amini A, Morris DL, Pourgholami MH. Significance of vascular endothelial growth factor in growth and peritoneal dissemination of ovarian cancer. Cancer Metastasis Rev 2012;31:143–62.
44. Peinado H, Zhang H, Matei IR, Costa-Silva B, Hoshino A, Rodrigues G, et al. Pre-metastatic niches: organ-specific homes for metastases. Nat Rev Cancer 2017;17:302–17.
45. Costa-Silva B, Aiello NM, Ocean AJ, Singh S, Zhang H, Thakur BK, et al. Pancreatic cancer exosomes initiate pre-metastatic niche formation in the liver. Nat Cell Biol 2015;17:816–26.
46. Wohlfeil SA, Hafele V, Dietsch B, Schledzewski K, Winkler M, Zierow J, et al. Hepatic endothelial notch activation protects against liver metastasis by regulating endothelial-tumor cell adhesion independent of angiocrine signaling. Cancer Res 2019;79:598–610.
47. Lee JW, Stone ML, Porrett PM, Thomas SK, Komar CA, Li JH, et al. Hepatocytes direct the formation of a pro-metastatic niche in the liver. Nature 2019;567:249–52.

48. Inverso D, Shi J, Lee KH, Jakab M, Ben-Moshe S, Kulkarni SR, et al. A spatial vascular transcriptomic, proteomic, and phosphoproteomic atlas unveils an angiocrine Tie-Wnt signaling axis in the liver. Dev Cell 2021;56:1677–93.

49. Hiratsuka S, Goel S, Kamoun WS, Maru Y, Fukumura D, Duda DG, et al. Endothelial focal adhesion kinase mediates cancer cell homing to discrete regions of the lungs via E-selectin upregulation. Proc Natl Acad Sci U S A 2011;108: 3725–30.

50. Alvarez-Martins I, Remedio L, Matias I, Diogo LN, Monteiro EC, Dias S. The impact of chronic intermittent hypoxia on hematopoiesis and the bone marrow microenvironment. Pflugers Arch 2016;468:919–32.

51. Dhillon AS, Hagan S, Rath O, Kolch W. MAP kinase signalling pathways in cancer. Oncogene 2007;26:3279–90.

52. Lu Z, Xu S. ERK1/2 MAP kinases in cell survival and apoptosis. IUBMB Life 2006;58:621–31.

53. Chen J, Fujii K, Zhang L, Roberts T, Fu H. Raf-1 promotes cell survival by antagonizing apoptosis signal-regulating kinase 1 through an MEK–ERK independent mechanism. Proc Natl Acad Sci U S A 2001;98:7783–8.

54. Nallapalli RK, Ibrahim MX, Zhou AX, Bandaru S, Sunkara SN, Redfors B, et al. Targeting filamin A reduces K-RAS–induced lung adenocarcinomas and endothelial response to tumor growth in mice. Mol Cancer 2012;11:50.

55. Zarubin T, Han J. Activation and signaling of the p38 MAP kinase pathway. Cell Res 2005;15:11–8.

56. Corre I, Paris F, Huot J. The p38 pathway, a major pleiotropic cascade that transduces stress and metastatic signals in endothelial cells. Oncotarget 2017;8: 55684–714.

57. Radu M, Semenova G, Kosoff R, Chernoff J. PAK signalling during the development and progression of cancer. Nat Rev Cancer 2014;14:13–25.

58. Ong CC, Jubb AM, Haverty PM, Zhou W, Tran V, Truong T, et al. Targeting p21-activated kinase 1 (PAK1) to induce apoptosis of tumor cells. Proc Natl Acad Sci U S A 2011;108:7177–82.

59. Schurmann A, Mooney AF, Sanders LC, Sells MA, Wang HG, Reed JC, et al. p21-activated kinase 1 phosphorylates the death agonist bad and protects cells from apoptosis. Mol Cell Biol 2000;20:453–61.

60. Wang J, Zhu Y, Chen J, Yang Y, Zhu L, Zhao J, et al. Identification of a novel PAK1 inhibitor to treat pancreatic cancer. Acta Pharm Sin B 2020;10:603–14.

61. Wang K, Huynh N, Wang X, Baldwin G, Nikfarjam M, He H. Inhibition of p21 activated kinase enhances tumour immune response and sensitizes pancreatic cancer to gemcitabine. Int J Oncol 2018;52:261–9.

62. Jambusaria A, Klomp J, Hong Z, Rafii S, Dai Y, Malik AB, et al. A computational approach to identify cellular heterogeneity and tissue-specific gene regulatory networks. BMC Bioinf 2018;19:217.

63. Schultze A, Fiedler W. Clinical importance and potential use of small molecule inhibitors of focal adhesion kinase. Anticancer Agents Med Chem 2011;11:593–9.

64. Jiang H, Hegde S, Knolhoff BL, Zhu Y, Herndon JM, Meyer MA, et al. Targeting focal adhesion kinase renders pancreatic cancers responsive to checkpoint immunotherapy. Nat Med 2016;22:851–60.

65. Stokes JB, Adair SJ, Slack-Davis JK, Walters DM, Tilghman RW, Hershey ED, et al. Inhibition of focal adhesion kinase by PF-562,271 inhibits the growth and metastasis of pancreatic cancer concomitant with altering the tumor microenvironment. Mol Cancer Ther 2011;10:2135–45.